

Supporting Information

NMR and Mössbauer Studies Reveal a Temperature-Dependent Switch from S = 1 to S = 2 in a Nonheme Oxoiron(IV) Complex with Faster C–H Bond Cleavage Rates

Waqas Rasheed^{†a}, Nabhendu Pal^{†a}, Ahmed M. Aboelenen^a, Saikat Banerjee^a, Williamson N. Oloo^a, Johannes E. M. N. Klein^a, Ruixi Fan^b, Jin Xiong^b, Yisong Guo^{*b}, and Lawrence Que, Jr^{*a}.

^a Department of Chemistry and Center of Metals in Biocatalysis, University of Minnesota Twin Cities, 207 Pleasant Street SE, Minneapolis, Minnesota 55455, United States

^b Department of Chemistry, Carnegie Mellon University, Pittsburgh, PA 15213, United States

E-mail: larryque@umn.edu

E-mail: ysguo@andrew.cmu.edu

Table of Contents

Section		Page No.
S-1	Instrumentation	3
S-2	Materials	3
S-3	Synthesis and Characterization of Oxidants, Ligands and Iron(II) Complexes	4-9
	A) General synthetic procedures for ligands	
	1) Ligand names and structures	
	2) Synthesis of substituted BQP(5Me)A ligand	
	3) Synthesis of substituted BQP(3Me)A ligand	
	4) Synthesis of substituted BQP*A ligand	
	B) Synthesis of iron(II) complexes	
	1) Synthesis of known iron(II) salts	
	2) Synthesis of [Fe ^{II} (BQP(5-Me)A)(OTf)]OTf	
	3) Synthesis of [Fe ^{II} (BQP(3-Me)A)(OTf)]OTf	
	4) Synthesis of [Fe ^{II} (BQP*A)(OTf)]OTf	
	C) ¹ H-NMR spectra of iron(II) complexes	
S-4	Synthesis and Characterization of Oxoiron(IV) Complexes	9-31
	A) Synthesis and in-situ generation of Oxoiron(IV) complexes	
	B) UV-vis spectroscopy of Oxoiron(IV) complexes	
	C) Reactivity and kinetic studies of Oxoiron(IV) complexes	
	D) NMR spectroscopy of complexes Oxoiron(IV) complexes	
	1) Generation of the oxoiron(IV) complexes for NMR spectroscopic analysis	
	2) General parameters for data collection and processing	
	3) Different structural configurations for pyridines in Complex 0	
	4) ¹ H-NMR spectra of [Fe ^{IV} (O)(N ₂ Py ₂ Q)] ²⁺	
	5) Patterns of shifts in S = 1 oxoiron(IV) complexes containing heterocycles) ¹ H-NMR spectra of oxoiron(IV) complexes and the corresponding decay product	
	E) Mössbauer spectroscopy of oxoiron(IV) complexes	
S-5	Calculated and Experimental NMR Paramagnetic Shifts	32-37
S-6	DFT Coordinates	37-40
S-7	References	41-42

1. Instrumentation

NMR (nuclear magnetic resonance) spectra for iron(II) complexes as well as iron(IV) complexes were recorded on a Bruker 400 or 500 MHz spectrometer at temperatures stated. NMR spectra to characterize the ligands were obtained at 298 K. 8" Wilmad-LabGlass 528-PP-7-5 NMR tubes were used to collect NMR spectra for iron(IV) and iron(II) complexes. For all the variable temperature spectra, the lower temperatures were calibrated using a sealed NMR tube containing a solution of tetramethylsilane (TMS) and methanol as a standard.

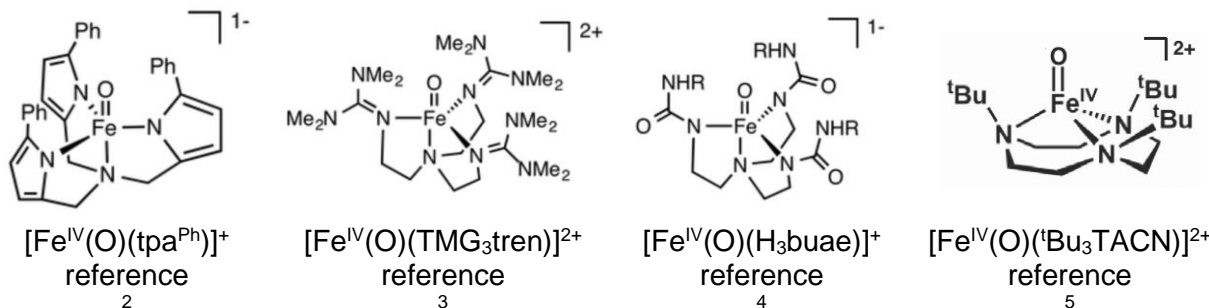
Elemental analyses were carried out by Atlantic Microlab (Norcross, GA).

UV-vis spectra and reactivity studies were recorded on a HP8453A diode array spectrometer equipped with a cryostat from Unisoku Scientific Instruments (Osaka, Japan).

Mössbauer spectra were recorded with two spectrometers, using Janis Research (Wilmington, MA) SuperVaritemp dewars that allow studies in applied magnetic fields of up to 7.5 T in the temperature range from 1.5 to 200 K. A LakeShore Model 331A temperature controller was used to control the temperature in experiments. Mössbauer spectral simulations were performed using the WMOSS software package (SEE Co, Edina, Minnesota). Isomer shifts are quoted relative to α -Fe metal at 298 K. The spectra were plotted by SpinCount developed by Prof. Michael Hendrich at Carnegie Mellon University.¹

2. Materials

All materials were bought from Sigma Aldrich, Fischer Scientific or TCI Chemicals, unless otherwise noted. The substrates cyclohexane, cyclooctane, toluene, ethylbenzene, cyclooctane and cumene used in kinetic experiments were passed through a plug of silica before use. All experiments to determine rate constants were carried out under nitrogen. Commercially available solvents like anhydrous acetonitrile, 2,2,2-trifluoroethanol (TFE) and deuterated dichloromethane, acetone and acetonitrile were used without further purification, unless otherwise noted. All oxygen- and moisture-sensitive compounds were synthesized in a nitrogen-filled glovebox.

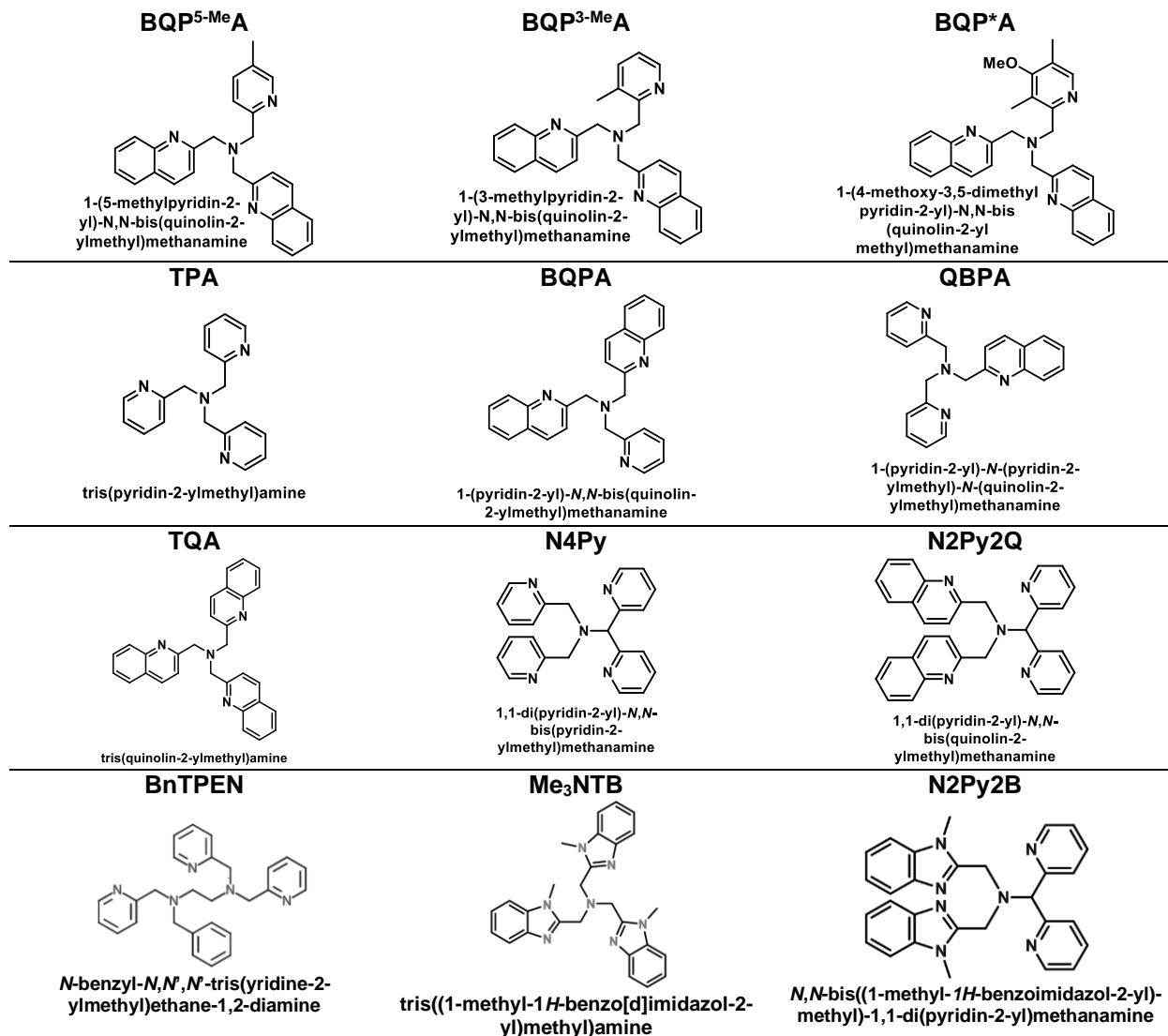


Scheme S1. Examples of $S = 2$ oxoiron(IV) complexes that are supported by trigonal arrangements of ligands

3. Synthesis and Characterization of Ligands, Oxidants, and Iron(II) Complexes

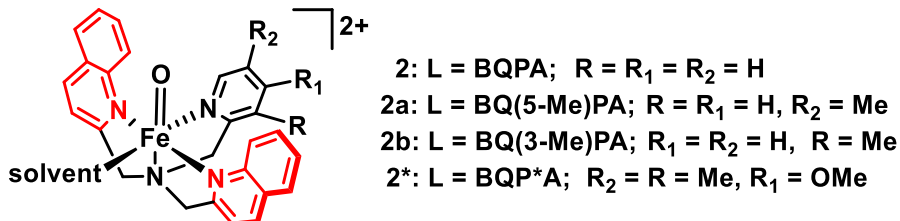
A) General synthetic procedures for ligands reported in this study

1. Ligand names and structures



Scheme S2. Names of TPA- and N4Py-based ligands examined in this study

Scheme S3 shows the BQPA-based ligands shown in Scheme S2 surrounding iron(IV) complexes and their corresponding names, in Scheme S2.



Scheme S3. Pyridine-ring-substituted variants of complex 2

2. Synthesis of ligand BQP(5-Me)A

2-(Aminomethyl)-5-methylpyridine⁶⁻⁸ (0.61g, 5 mmol) was added to a suspension of 2-chloromethylquinoline hydrochloride (2.14 g, 10 mmol) in anhydrous CH₃CN (30 ml). The mixture was treated with anhydrous K₂CO₃ (2.8 g, 20.2 mmol) and refluxed at 45 °C. After 3 days, the reaction mixture was cooled down to room temperature and filtered to remove any unreacted K₂CO₃ and KCl salt formed and. The solvent was then evaporated under vacuum to yield yellow solids, which were recrystallized from diethyl ether (yield 83 %).

¹H-NMR (400 MHz, CD₂Cl₂): 2.32 (3H, 5-CH₃), 3.90 (2H, py-CH₂), 4.10 (4H, Q-CH₂), 7.50-7.57 (m, 4H), 7.71 (t, 2H), 7.78 (d, 2H), 7.84 (d, 2H), 8.00 (d, 2H), 8.18 (d, 2H), 8.38 (d, 1H). ¹³C NMR (100 MHz, CD₂Cl₂): 159.5 ppm, 159.3 ppm, 148.99 ppm, 146.19 ppm, 136.21 ppm, 136.02 ppm, 135.52 ppm, 131.44 ppm, 130.10 ppm, 128.64 ppm, 127.36 ppm, 126.35 ppm, 123.10 ppm, 121.94 ppm, 121.11 ppm, 60.93 ppm, 60.37 ppm, 21.22 ppm. ESI-MS (in MeOH): obsd (calcd) for [BQP^{3-Me}A +H]⁺: m/z 405.3 (405.21).

3. Synthesis of ligand BQP(3-Me)A

2-(Aminomethyl)-3-methylpyridine⁶⁻⁸ (0.61g, 5 mmol) was added to a suspension of 2-chloromethylquinoline hydrochloride (2.14 g, 10 mmol) in anhydrous CH₃CN (30 ml). The mixture was treated with anhydrous K₂CO₃ (2.8 g, 20.2 mmol) and refluxed at 45 °C. After 3 days, the reaction was cooled down to room temperature, and filtered to remove KCl salt and unreacted K₂CO₃. The solvent was then removed to yield a yellow solid that was recrystallized from diethyl ether (yield 87 %).

¹H-NMR (400 MHz, CD₂Cl₂): 2.22 (3H, 3-CH₃), 3.95 (2H, py-CH₂), 4.00 (4H, Q-CH₂), 7.08 (t, 1H), 7.41 (d, 1H), 7.53 (t, 2H), 7.61 (d, 2H), 7.70 (t, 2H), 7.82 (d, 2H), 8.04 (d, 2H), 8.12 (d, 2H), 8.37 (d, 1H). ESI-MS (in MeOH): obsd (calcd) for [BQP^{5-Me}A +H]⁺: m/z 405.3 (405.21).

4. Synthesis of BQP^{*}A

2-(Aminomethyl)-3,5-dimethyl,4-methoxypyridine⁶⁻⁸ (1.66 g, 10 mmol) was added to a suspension of 2-chloromethylquinoline hydrochloride (4.28 g, 20 mmol) in anhydrous CH₃CN (30 ml). The mixture was treated with anhydrous K₂CO₃ (2.8 g, 20.2 mmol) and refluxed at 45 °C. After 3 days, the reaction was cooled down to room temperature, and then filtered to remove KCl salt and unreacted K₂CO₃. The solvent was then removed to yield yellow solids, which was then recrystallized from diethyl ether (yield 90 %).

¹H-NMR (400 MHz, CD₂Cl₂): 2.10 (3H, 3-CH₃), 2.16 (3H, 5-CH₃), 3.61 (3H, 4-MeO), 3.98 (2H, Py-CH₂), 4.06 (4H, Q-CH₂), 7.50 (t, 2H), 7.57 (d, 2H), 7.68 (t, 2H), 7.71 (d, 2H), 8.00 (m, 4H), 8.17 (d, 1H). ¹³C NMR (100 MHz, CD₂Cl₂): 163.95 ppm, 160.3 ppm, 156.55 ppm, 148.34 ppm, 147.50 ppm, 135.81 ppm, 129.14 ppm, 129.03 ppm, 127.46 ppm, 127.27 ppm, 126.15 ppm, 126.01 ppm, 125.21 ppm, 121.63 ppm, 61.93 ppm, 59.60 ppm, 12.90 ppm, 10.75 ppm. ESI-MS (in MeOH): obsd (calcd) for [BQP^{*}A+H]⁺: m/z 449.3 (449.23).

B) General synthetic procedures for iron(II) complexes

1) Synthesis of iron(II) complex [Fe^{II}(BQP(5-Me)A)](OTf)₂

To a solution of Fe(OTf)₂•2CH₃CN (97.0 mg, 0.220 mmol) in 1 mL anhydrous CH₃CN inside an inert glovebox, 1 equiv. BQP^{5Me}A (89.0 mg, 0.220 mmol) in 3 mL CH₃CN was added, and the mixture was stirred for three hours to give a yellowish green solution. This solution was then filtered and poured into a diethyl ether bath to produce a yellowish green precipitate, which was filtered again and washed with diethyl ether, to give a yellow-colored solid. This solid was re-dissolved in acetonitrile and crystallized by vapor diffusion using diethyl ether to give yellow crystals. (125 mg, 75 % yield). ¹H NMR (400 MHz, CD₃CN, 25 °C): δ (ppm) 117.8 (1H; α-H Py), 100.9 (2H; CH₂ Py), 57.7 (4H; CH₂ quin), 53.5 (2H; 7-H quin), 48.3 (1H; β'-H py), 22.3 (2H; 5-H Qn), 11.43 (2H; 3-H Qn), 2.7 (2H; 6-H Qn), 0.6 (3H; 5-Me Py), -3.30 (2H; 4-H quin), -6.70 (1H; γ-H Py), -58.33 (2H; 8-H Qn). Anal. calcd. for C₃₀H_{28.5}F₆FeN_{4.5}O_{7.5}S₂ corresponding to the complex Fe^{II}(BQP(5-Me)A)(OTf)₂•1.5H₂O•0.5CH₃CN: C, 44.70; H, 3.56; N, 7.82. Found: C, 44.66; H, 3.53; N, 7.33. ESI-MS (in MeCN): obsd (calcd) for [Fe^{II}(BQP(5-Me)A)(OTf)]⁺: m/z 609.01 (609.09).

2) Synthesis of iron(II) complex [Fe^{II}(BQP(3-Me)A)(OTf)₂]

To a solution of Fe(OTf)₂•2CH₃CN (75.0 mg, 0.170 mmol) in 1 mL anhydrous CH₃CN inside an inert glovebox was added 1 equiv. BQP^{3Me}A (68.8 mg, 0.170 mmol) in 2 mL CH₃CN and the mixture was stirred for three hours to give a yellowish green solution. This solution was then filtered and poured into a diethyl ether bath to produce a yellowish green precipitate, which was filtered again and washed with diethyl ether, to give a yellow-colored solid. This solid was re-dissolved in acetonitrile and crystallized by vapor diffusion using diethyl ether to afford yellow crystals. (100 mg, 78 % yield). ¹H NMR (400 MHz, CD₃CN, 25 °C): δ (ppm) 109.3 (1H; α-H py), 84.5 (2H; CH₂ Py), 60, 65 (4H; CH₂ quin), 54.2 (1H; β-H py), 51.1 (2H; 7-H quin), 22.6 (2H; 5-H quin), 7.6 (2H; 3-H quin), 3.1 (2H; 6-H quin), -1.7 (3H; 3Me Py) -4.77 (2H; 4-H quin), -4.70 (1H; γ-H py), -52.33 (2H; 8-H quin). Anal. calcd. for C₂₉H₂₆F₆FeN₄O₇S₂ representing Fe^{II}(BQP(3-Me)A)(OTf)₂•H₂O: C, 44.86; H, 3.37; N, 7.22. Found: C, 44.66; H, 3.53; N, 7.33. ESI-MS (in MeCN): obsd (calcd) for [Fe^{II}(BQP³-MeA)(OTf)]⁺: m/z 609.30 (609.09).

3) Synthesis of iron(II) complex [Fe^{II}(BQP^{*}A)(OTf)₂]

To a solution of Fe(OTf)₂•2CH₃CN (195 mg, 0.442 mmol) in 2 mL anhydrous CH₃CN inside an inert glovebox was added 1 equiv. BQP^{*}A (200 mg, 0.443 mmol) in 4 mL CH₃CN, and the mixture was stirred for three hours to give rise to a yellow solution. This solution was then filtered and poured into a diethyl ether bath to produce a yellowish green precipitate, which was filtered again and washed with diethyl ether, to give a yellow-

colored solid. This solid was re-dissolved in acetonitrile and crystallized by vapor diffusion using diethyl ether to give yellow crystals. (302 mg, 85 % yield). ^1H NMR (400 MHz, CD_3CN , 25 °C): δ (ppm) 111.5 (1H; α -H py), 92.3 (2H; CH_2 Py), 61.1 (4H; CH_2 quin), 51.7 (2H; 7-H quin), 22.2 (2H; 5 -H quin), 11.8 (2H; 3-H quin), 3.14 (2H; 6-H quin), 1.5 (3H; 4-MeO py), -0.7 (3H; 5-Me Py), -3.2 (3H; 3-Me Py), -51.3 (2H; 8-H quin) Anal. calcd. for $\text{C}_{31}\text{H}_{31}\text{F}_6\text{FeN}_4\text{O}_{8.5}\text{S}_2$ representing $\text{Fe}^{II}(\text{BQP}^*\text{A})(\text{OTf})_2 \cdot 1.5\text{H}_2\text{O}$: C, 44.88; H, 3.60; N, 6.75. Found: C, 48.30; H, 3.60; N, 6.66. ESI-MS (in MeCN): obsd (calcd) for $[\text{Fe}^{II}(\text{BQP}^*\text{A})(\text{OTf})]^+$: m/z 609.01 (609.09).

4) Synthesis of previously reported iron(II) complexes

Previously reported iron(II) complexes include those supported by their known ligands TPA⁹, QBPA¹⁰, BQPA¹⁰, TQA¹¹, N2Py2Q¹², and N4Py.¹³ In their syntheses, the only change was that iron(II) triflate was used instead of iron(II) perchlorate, in order to mitigate the risks associated with the explosive nature of perchlorates.

Other $^{57}\text{Fe}^{II}$ -labeled complexes were synthesized using the same synthetic procedures as above, except that $^{57}\text{Fe}^{II}(\text{CH}_3\text{CN})_2(\text{OTf})_2$ was used on a 10-20 mg scale as the iron(II) triflate starting material. Details for the preparation of oxoiron(IV) solutions for Mössbauer spectroscopy are detailed in the Mössbauer section.

C) $^1\text{H-NMR}$ spectra of iron(II) complexes

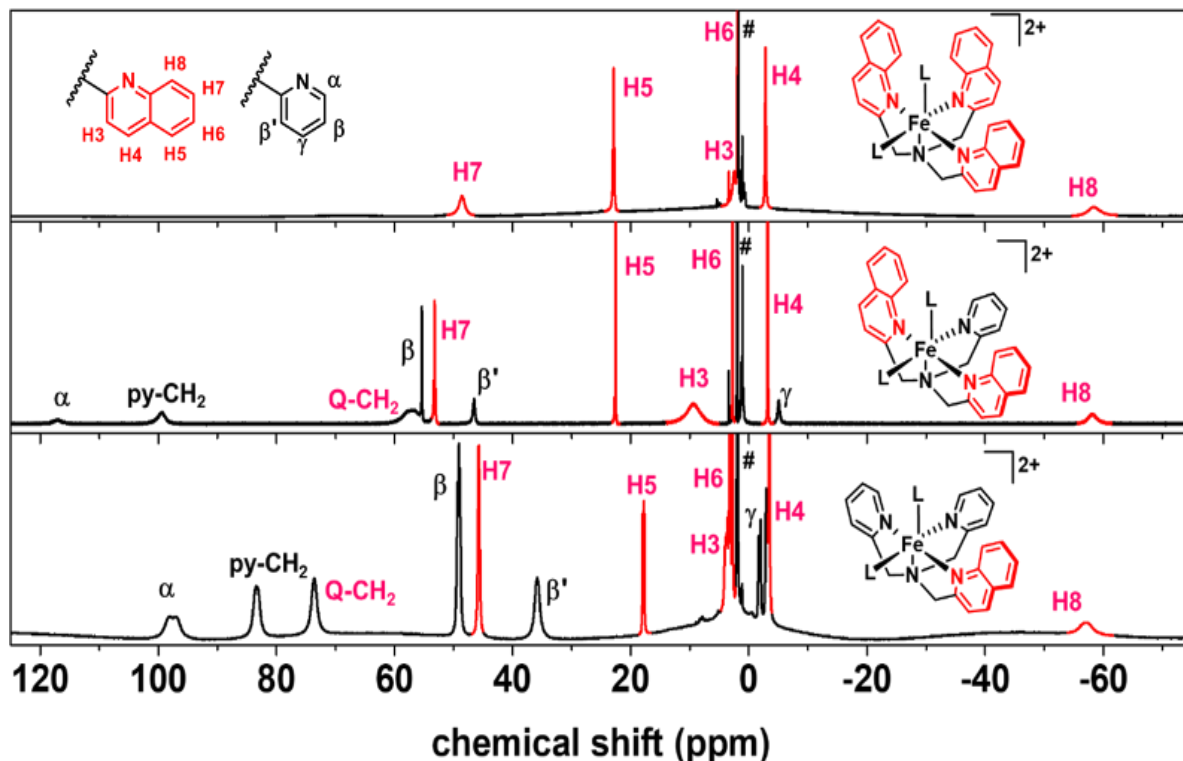


Figure S1. ^1H -NMR spectra of iron(II) complexes obtained at 298 K in acetonitrile- d_3 (residual CH_3CN peaks from the solvent denoted by #).¹⁰

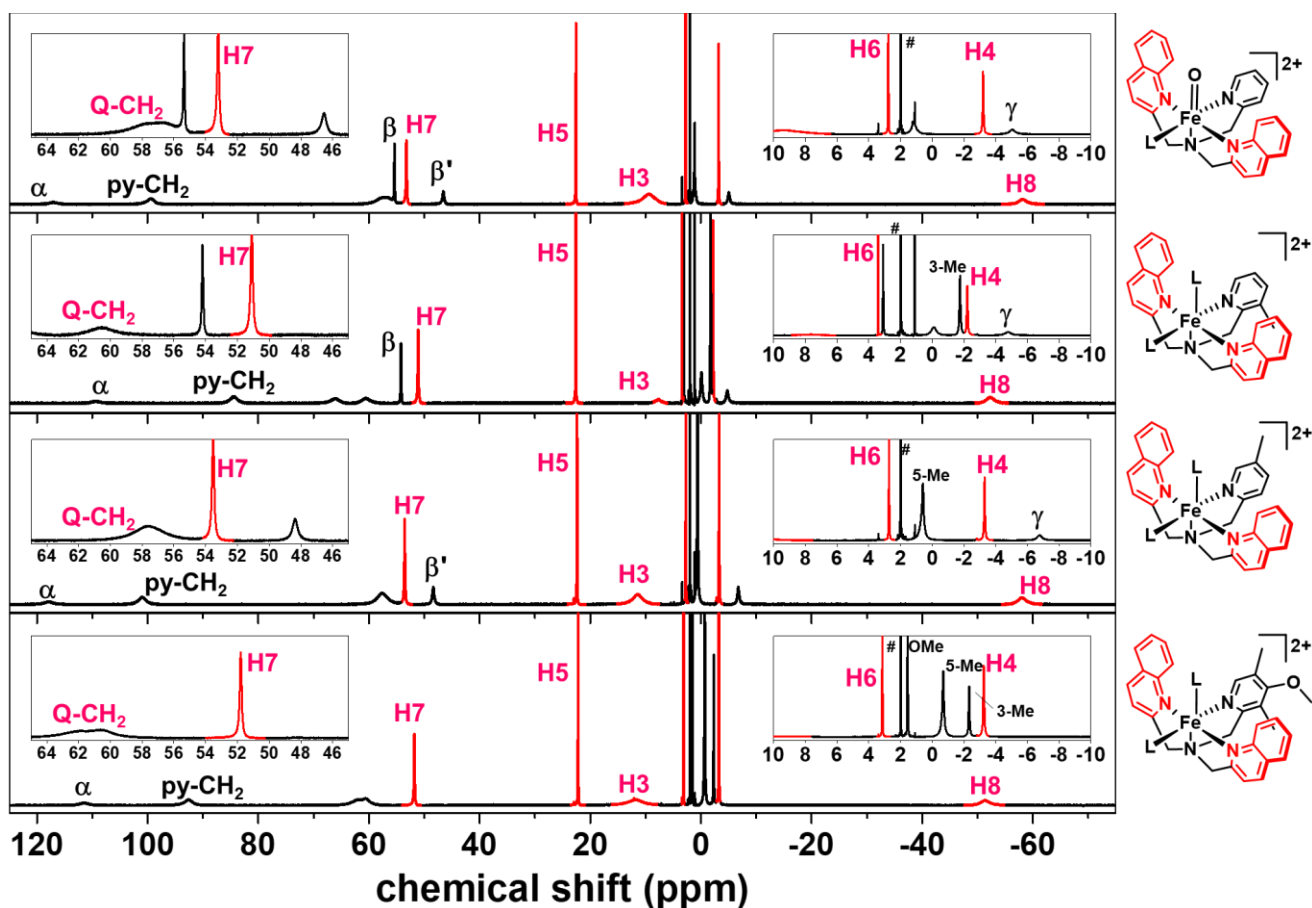


Figure S2. ^1H -NMR spectra of iron(II) complexes of substituted BQPA ligands obtained at 298 K in acetonitrile- d_3 (residual CH_3CN peaks from the solvent denoted by #). Insets show selected magnified sections of the spectra. See Figure S1 for quin/py H labels

Notes on assignments of ^1H NMR signals in solutions of iron(II) complexes:

The β , β' and γ signals are assigned based on comparisons with the NMR spectra of $[\text{Fe}^{II}(6\text{MeTPA})(\text{L})_n]^{2+}$ and $[\text{Fe}^{II}(6\text{Me}_3\text{TPA})(\text{L})_n]^{2+}$ complexes.⁹ These signals can also be assigned based on changes observed upon substitution of these protons with methyl and methoxy groups. Quinoline H4 and pyridine γ -H protons give rise to similarly shifted signals, likely due to the similar paramagnetic effects experienced by these protons on their respective heterocycles. H5, H6 and H7 are the farthest from the paramagnetic center and thus have the sharpest signals, with H6 being the sharpest followed by H5 and then H7. This also follows from their expected relative proximity to the iron center. H8 is likely to be very broad and tentatively assigned to upfield signals from -50 to -60 ppm.

Table S1. ^1H NMR chemical shifts for iron(II) complexes at 298 K in CD_3CN . FWHM given in parentheses. Italicized values are for methyl/methoxy protons.

protons	BQPA	BQP* A	BQP(5-Me) A	BQP(3-Me) A
α -H Py	116.8 (740)	111.5 (750)	117.8 (780)	109.35 (810)
β -H Py	55.37 (43)	<i>-0.7 (5-Me)</i> (96)	<i>0.6 (5-Me)</i> (64)	54.20 (63)
β' -H Py	46.5 (155)	<i>-3.2 (3-Me)</i> (71)	48.3 (180)	<i>-1.70 (3-Me)</i> (51)
γ -H Py	-5.1 (160)	<i>1.5 (OMe)</i> (20)	-6.7 (160)	-4.7 (200)
CH_2 Py	99.3 (620)	92.3 (580)	100.9 (640)	84.50 (760)
H3	9.49 (740)	11.8 (1200)	11.43 (880)	7.64 (420)
H4	-3.2 (36)	-2.3 (70)	-3.3 (35)	-4.77 (200)
H5	22.6 (29)	22.2 (66)	22.3 (27)	22.6 (44)
H6	2.76 (27)	3.14 (63)	2.7 (22)	3.10 (35)
H7	53.2 (68)	51.7 (96)	53.5 (67)	51.1 (65)
H8	-58.1 (670)	-51.3 (810)	-58.0 (720)	-52.33 (680)
CH_2 -Q	56.9 (1400)	61.1 (1100)	57.7 (580)	60 (720), 66 (780)

In Table S1, β' -H signals are broader compared to β -H signals, as indicated by their FWHMs in the parent iron(II) complex supported by BQPA. Similarly, the β' -H signal of iron(II) complex supported by BQP(5-Me)**A** is broader than the β -H signal in iron(II) complex supported by BQP(3-Me)**A**. This is also true for $S = 1$ iron(IV) complexes, and would be expected to be true for $S = 2$ iron(IV) complexes, as FWHM has to do with proximity to the iron center, and β' -H are generally closer to it than β -H (in Tables S5-6).

4. Synthesis & Characterization of Oxoiron(IV) Complexes

A) Synthesis and/or *in-situ* generation of oxoiron(IV) complexes

All oxoiron(IV) complexes supported by tripodal ligands in this study were generated at given temperatures by treatment of solutions of their iron(II) precursors of given concentration in appropriate solvents with 1-2 equivalents of oxidant ArIO . These solutions were used for reactivity studies or to obtain NMR, UV-visible or Mössbauer spectra. Details are given in the relevant section for sample preparation and each

spectroscopic measurement. the sequential replacement of pyridines in $[\text{Fe}^{\text{IV}}(\text{O})(\text{TPA})(\text{MeCN})]^{2+}$ (**0**) with sterically bulkier quinolines to form the complexes $[\text{Fe}^{\text{IV}}(\text{O})(\text{QBPA})(\text{MeCN})]^{2+}$ (**1**), $[\text{Fe}^{\text{IV}}(\text{O})(\text{BQPA})(\text{MeCN})]^{2+}$ (**2**), and $[\text{Fe}^{\text{IV}}(\text{O})(\text{TQA})(\text{MeCN})]^{2+}$ (**3**). Of these complexes,¹⁴⁻¹⁷ only **2** has not been previously reported. The oxoiron(IV) complexes supported by pentadentate ligands were generated as previously reported.^{12, 18}

B) UV-vis spectroscopy of oxoiron(IV) complexes

All samples were generated in 1-cm quartz cells at appropriate temperatures using 1 mL of 1-mM iron(II) solutions in acetonitrile, to which 2 equivalents of ArIO dissolved in either 2,2,2-trifluoroethanol or dichloromethane-*d*₂ was added. Their generation was followed using UV-vis spectroscopy at given temperatures using the cryostat-equipped UV-visible spectrophotometer, to stabilize and lower the temperature using liquid from a dewar.

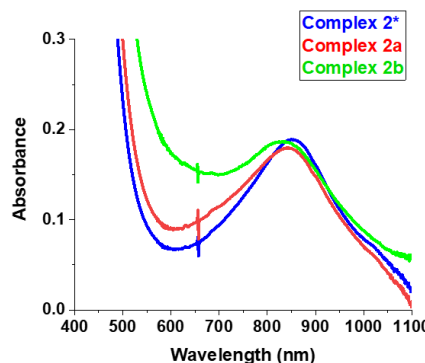


Figure S3. UV-vis spectra of **2**, **2a**, **2b** and **2***, in acetonitrile at 233 K, obtained by adding 2 equiv ArIO in CD_2Cl_2 to 1-mM iron(II) solutions. Instrument artifact at ≈ 660 nm.

Table S2. Spectroscopic and stability properties of substituted oxoiron(IV) variants of **2**.

Complex	2	2a	2b	2*
λ_{max} (nm)	840	840	834	855
Half-life* (min)	2	4	3	2.5

Samples were generated at 233 K from 1-mM solutions of the Fe(II) precursor in acetonitrile upon treatment with 2 eq ArIO dissolved in $\text{DCM}-d_2$.

C) Reactivity and kinetic studies of oxoiron(IV) complexes

All experiments were conducted with 1-1.5 mL solutions of 1 mM iron(II) complexes in MeCN solutions at given temperatures for HAT (hydrogen-atom-transfer) substrates. The oxoiron(IV) complexes were generated using 1-2 eq. ArIO in 2,2,2-trifluoroethanol or DCM-*d*₂. The pseudo-first order decay curves from absorption-time profiles were obtained by monitoring the decrease in absorbance for the oxoiron(IV) complexes with time, from their absorbance spectra, when a known concentration of substrate is introduced. These

profiles at various concentrations of substrates were fit with a first order exponential decay equation. The rates obtained (k_{obs}) were then plotted against different concentrations of substrates, and their slopes represent 2nd order rate constants (k_2).

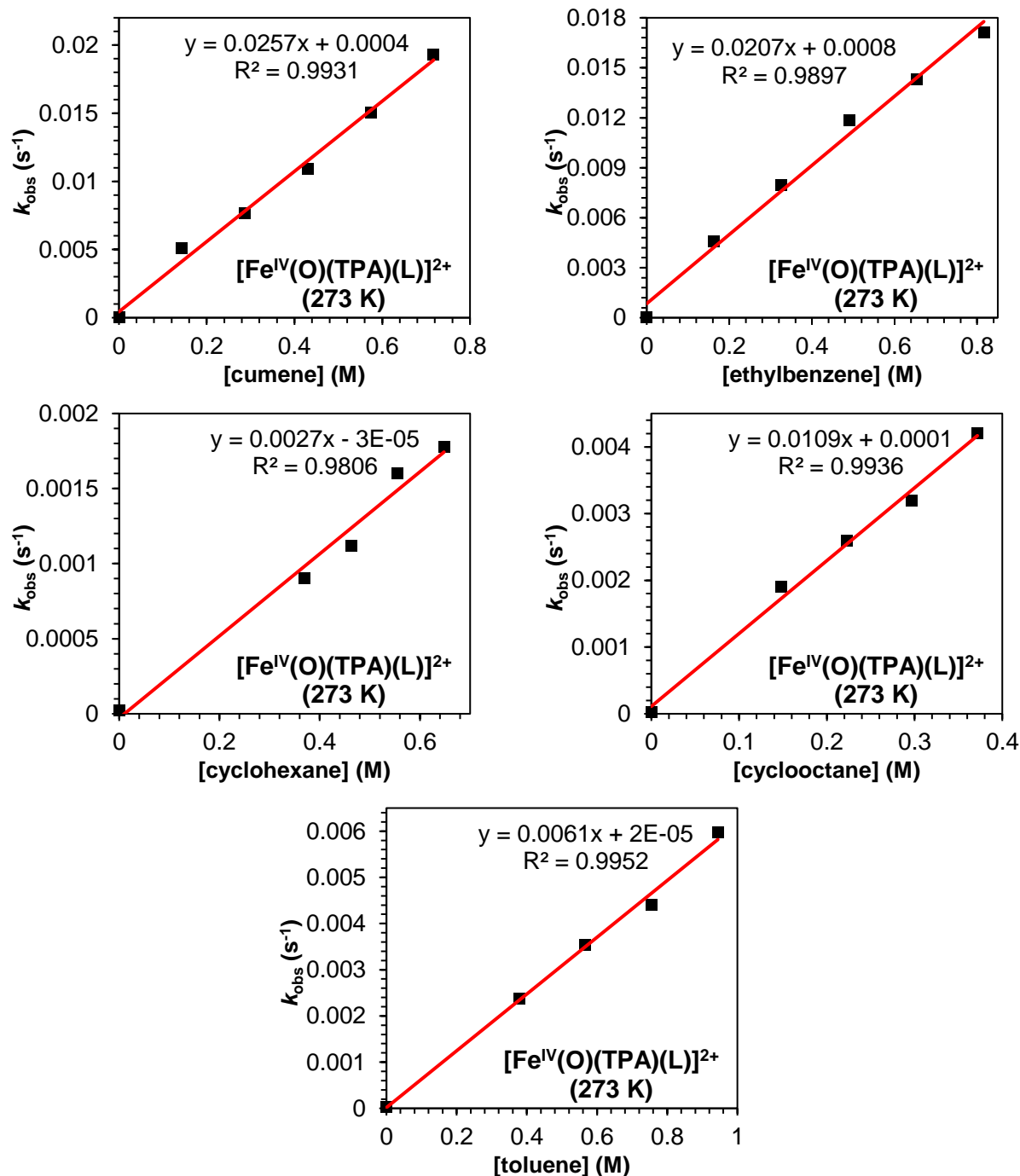


Figure S4. k_2 plots for the reactions of various HAT substrates with $[\text{Fe}^{\text{IV}}(\text{O})(\text{TPA})(\text{L})]^{2+}$ (0). The slopes of the fitted red lines represent the second-order rate constants (k_2) at 273 K. The oxoiron(IV) complex was generated by adding 1.2 eq s-ArIO in TFE to a MeCN solution of the iron(II) complex.

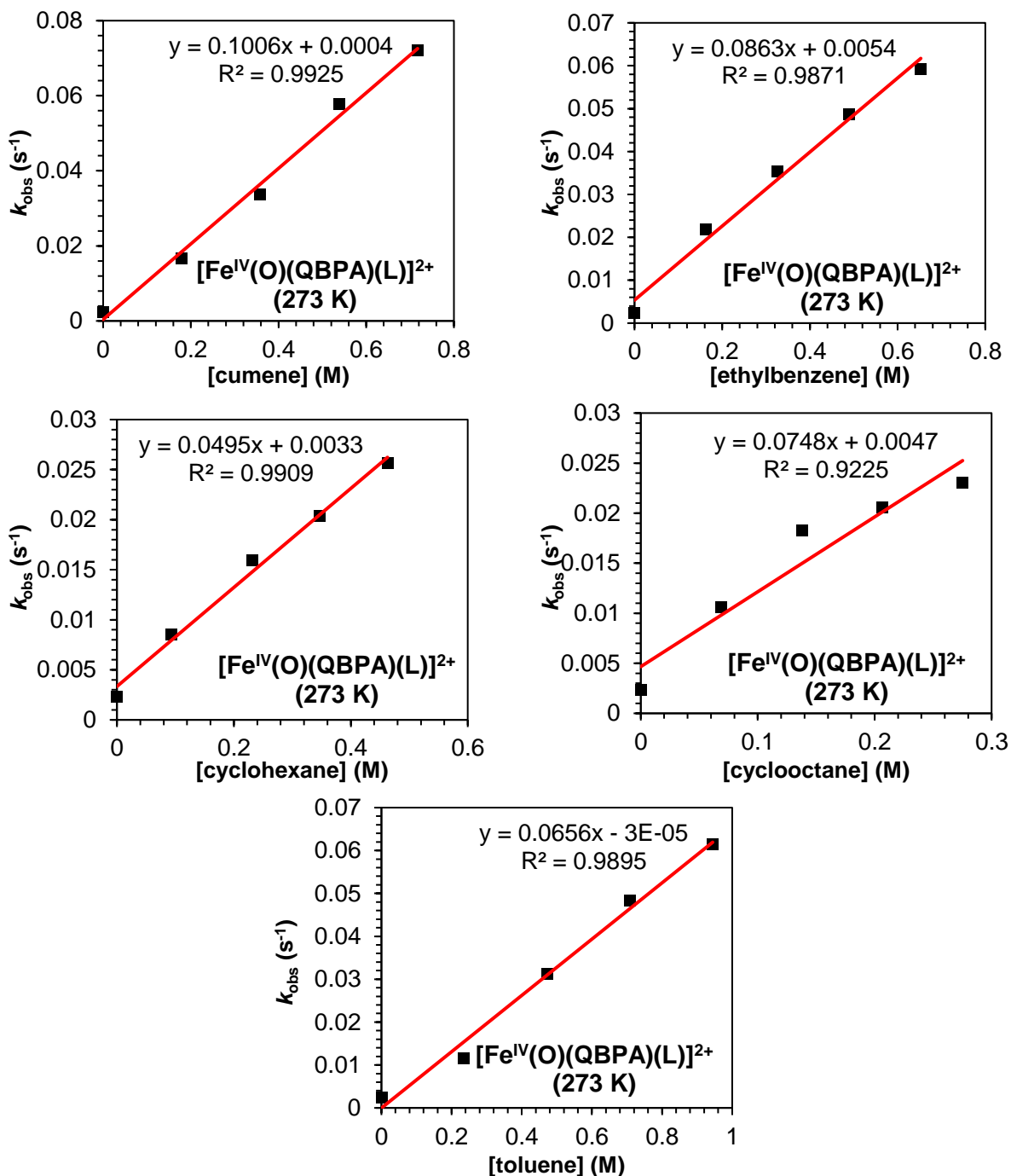


Figure S5. k_2 plots for the reactions of different HAT substrates with $[\text{Fe}^{\text{IV}}(\text{O})(\text{QBPA})(\text{L})]^{2+}$ (**1**) in MeCN. The slopes of the fitted red lines represent the second-order rate constants (k_2) at 273 K. The oxoiron(IV) complex was formed with 1.2 eq s-ArIO.

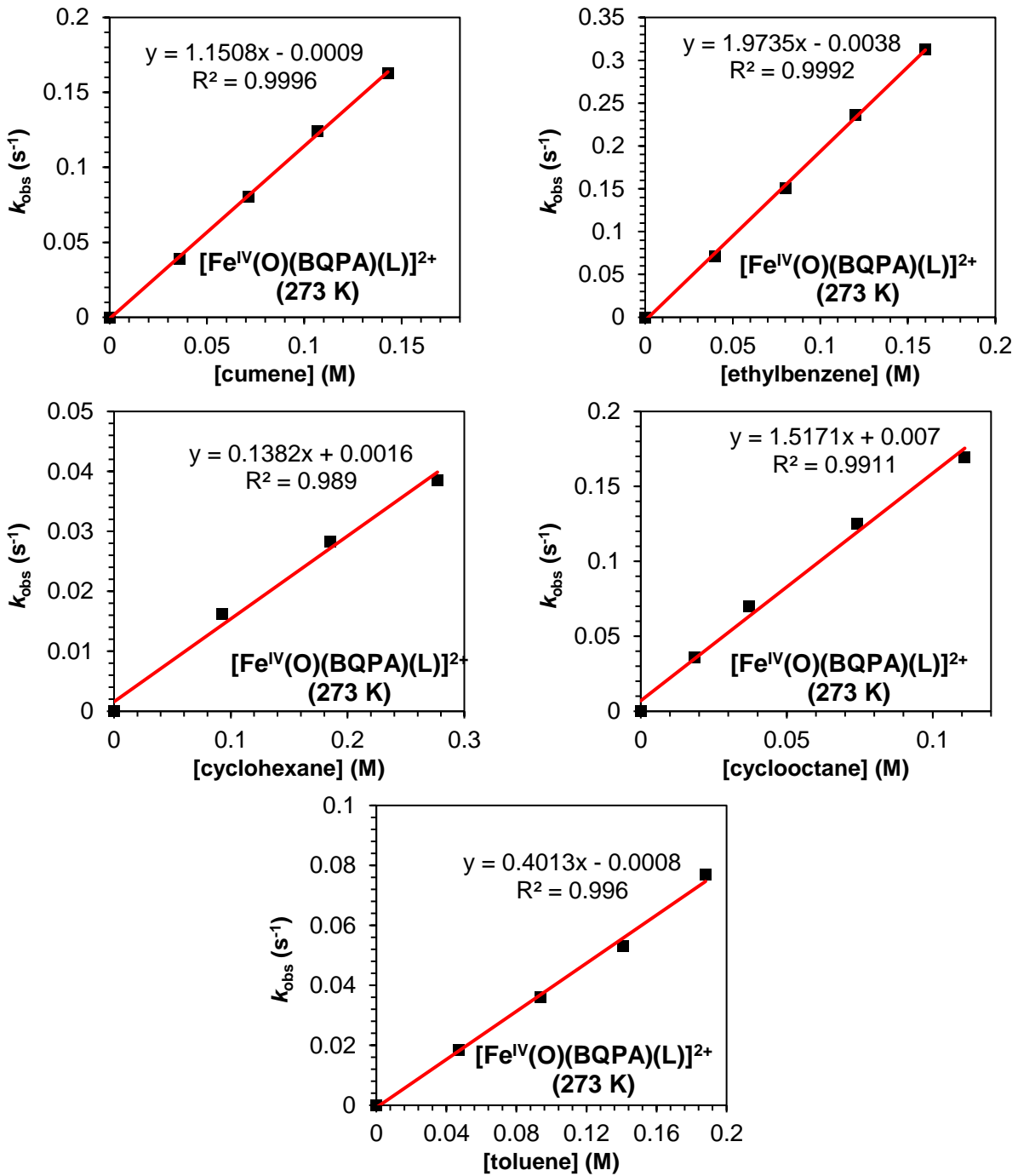


Figure S6. k_2 plots for the reactions of different HAT substrates with $[\text{Fe}^{\text{IV}}(\text{O})(\text{BQPA})(\text{L})]^{2+}$ (2). The slopes of the fitted red lines represent the second-order rate constants (k_2) at 233 K. The oxoiron(IV) complex was generated using 2 eq s-ArIO followed by addition of substrate, except for cyclooctane and cyclohexane where the substrate was dissolved first before adding the oxidant.

Table S3. Summary of 2nd-order rate constants (k_2) for oxoiron(IV) complexes, as derived from the plots in Figures S4 through S6. HAT rates were measured under N₂ at given temperatures.

Substrate	D _{C-H} (kcal/mol)	N2Py2Q (298 K)	TPA (0) (273 K)	QBPA (1) (273 K)	BQPA (2) (233 K)	TQA (3) (233 K)
Cumene	84.5	0.16	0.026 ± 0.001	0.1 ± 0.005	1.15 ± 0.014	1
Ethylbenzene	87	0.1	0.021 ± 0.001 0.0028 ± 0.00005 (233 K)	0.086 ± 0.006 0.01 ± 0.0005 (233 K)	1.97 ± 0.03	2.1
Toluene	90	0.012	0.0061 ± 0.0002	0.065 ± 0.004	0.40 ± 0.015	0.64
Cyclooctane	95.3	0.13	0.011 ± 0.0005	0.075 ± 0.012	1.5 ± 0.08	3.5
Cyclohexane	99.3	0.029	0.0027 ± 0.0002	0.05 ± 0.003	0.13 ± 0.01	0.37
approx. t_{1/2} (min)		150	460	40	2	15
reference		¹²	This work	This work	This work	¹⁹

Table S4. Summary of 2nd-order rate constants (k'_2 , normalized per equivalent C–H bond present on substrate) for TPA-based complexes, as derived from the plots in Figures S4 through S6. HAT rates were measured under N₂ at given temperatures.

Substrate	D _{C-H} (kcal/mol)	N2Py2Q (298 K)	TPA (0) (273 K)	QBPA (1) (273 K)	BQPA (2) (233 K)	TQA (3) (233 K)
Cumene	84.5	0.16	0.026	0.10	1.15	1
Ethylbenzene	87	0.05	0.011	0.043	0.98	1.05
Toluene	90	0.004	0.0020	0.022	0.13	0.21
Cyclooctane	95.3	0.0081	0.00069	0.0047	0.094	0.22
Cyclohexane	99.3	0.0024	0.00023	0.0042	0.011	0.031

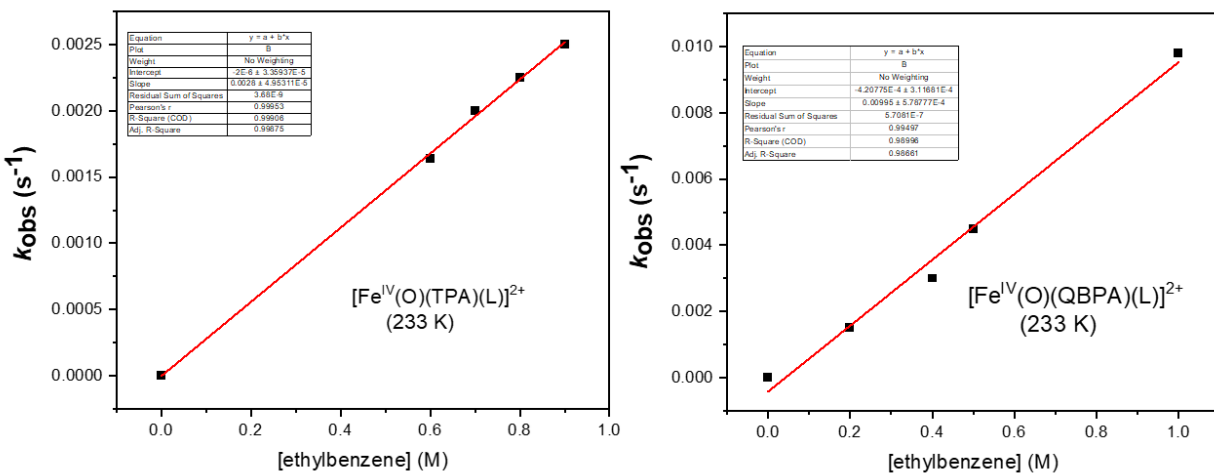


Figure S7. k_2 plots for the reactions of ethylbenzene with $[\text{Fe}^{\text{IV}}(\text{O})(\text{TPA})(\text{L})]^{2+}$ and $[\text{Fe}^{\text{IV}}(\text{O})(\text{QBPA})(\text{L})]^{2+}$. The slopes of the fitted red lines represent the second-order rate constants (k_2) at 233 K. The oxoiron(IV) complex was generated using 2 eq s-ArIO followed by addition of substrate.

D) NMR spectroscopy of oxoiron(IV) complexes

1) Generation of the ferryl complexes for NMR spectroscopic analysis

4-mM stock solutions of starting iron(II) precursors were made within an air-free nitrogen-filled glovebox in acetonitrile- d_3 or acetone- d_6 . Samples of the oxoiron(IV) complexes for NMR analysis were generated by transferring 0.5 mL of a precursor solution into an NMR tube (in glove box) and cooling it to the desired temperature in the NMR instrument for analysis; at this point a ^1H NMR spectrum of the iron(II) precursor was obtained, after locking to the residual proton signal in the deuterated solvent, tuning to the intended nucleus, and then shimming to obtain a uniform magnetic field around the sample. The following three steps were then performed in quick succession: 1) the NMR tube was ejected from the instrument, 2) 2 equivalents of ArIO in either 2,2,2-trifluoroethanol (TFE) or DCM- d_2 were quickly injected to generate the oxoiron(IV) intermediate; the tube was recapped with either a septum or its plastic cap (to minimize decay of the species) and 3) the tube was immediately inserted back into the instrument for data collection. Because the instrument had been locked to the solvent as well as tuned to the nucleus of interest, only quick shimming was performed again before collection of NMR data for the oxoiron(IV) species. To obtain the spectrum of the decayed species, the complex was warmed to room temperature by ejecting the NMR tube from the instrument, and after the species had decayed, it was inserted back into the instrument and NMR data was obtained again at a lowered temperature.

2) General parameters for data collection and processing

The following parameters were used to acquire the ^1H NMR data for paramagnetic compounds: acquisition time = 0.064 s; relaxation delay = 0.03 s; sweep width = 400 ppm offset (centered) at 6 ppm; line broadening factor = 10-30 Hz. Chemical shifts (ppm) were referenced to residual protic solvent peaks. The NMR spectra obtained were processed using the NMR processing software MestReNova 12.0 or Bruker's Top-Spin 3.5pl7.

3) Consequences of having different structural configurations of pyridines around the Fe=O unit.

For the 6-coordinate complex **0**, there are two possible configurations with respect to the oxo unit, either it is trans to the tertiary amine (more commonly observed) or trans to one of the three pyridines and cis to the other two pyridines with planes oriented perpendicular to the $\text{Fe}^{\text{IV}}=\text{O}$ unit. The DFT-predicted $^1\text{H-NMR}$ shifts for the pyridine-H signals of the latter isomer span a range of only 20 to -10 ppm, a prediction confirmed in the $^1\text{H-NMR}$ spectrum of $[\text{Fe}^{\text{IV}}(\text{O})(\text{BnTPEN})]^{2+}$ ($\text{BnTPEN} = \text{N-benzyl-}N',N',N'\text{-tris(2-pyridylmethyl)-1,2-diaminoethane}$) in which the pyridine with its plane perpendicular to the Fe=O unit exhibits resonances at 8 ppm for the γ -H and at -0.2 and -2.0 ppm for the β -H's. However, the $^1\text{H-NMR}$ spectrum of complex **0** obtained at 233 K does not exhibit such a small range of shifts predicted for this hypothetical isomer, thus ruling out this possible isomer. Instead, a set of peaks similar to that seen for $[\text{Fe}^{\text{IV}}(\text{O})(\text{N}4\text{Py})]^{2+}$ is observed, indicating that there is no pyridine in **0** that is bound with its plane perpendicular to the Fe=O unit.

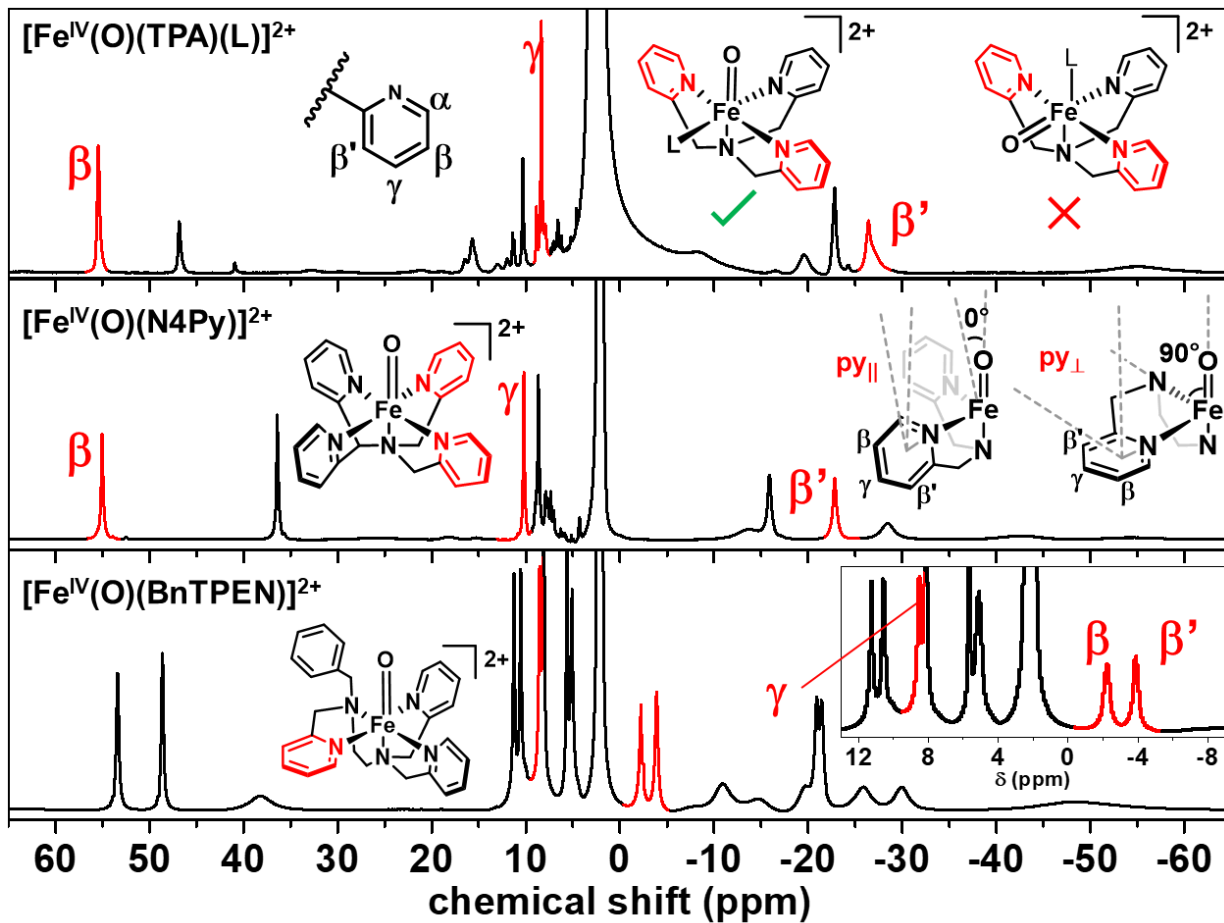


Figure S8. ^1H -NMR spectra of various complexes that establish the solution state structure of complex **0** (top panel) at 233 K in CD_3CN . The red highlighted peaks belong to the red pyridines. The NMR shift patterns for any pyridine in **0** do not match the NMR patterns observed for the pyridine perpendicular to the oxoiron(IV) unit in $[\text{Fe}^{\text{IV}}(\text{O})(\text{BnTPEN})]^{2+}$ (bottom panel), thus ruling out any solution-state configuration for **0** where a pyridine is perpendicular to the oxoiron(IV) unit. However the peaks observed do match shift patterns found in $[\text{Fe}^{\text{IV}}(\text{O})(\text{N}4\text{Py})]^{2+}$ (middle panel) where all the pyridines are aligned roughly parallel to the oxoiron(IV) unit.

4) NMR spectra for $[\text{Fe}^{\text{IV}}(\text{O})(\text{N}2\text{Py}2\text{Q})]^{2+}$

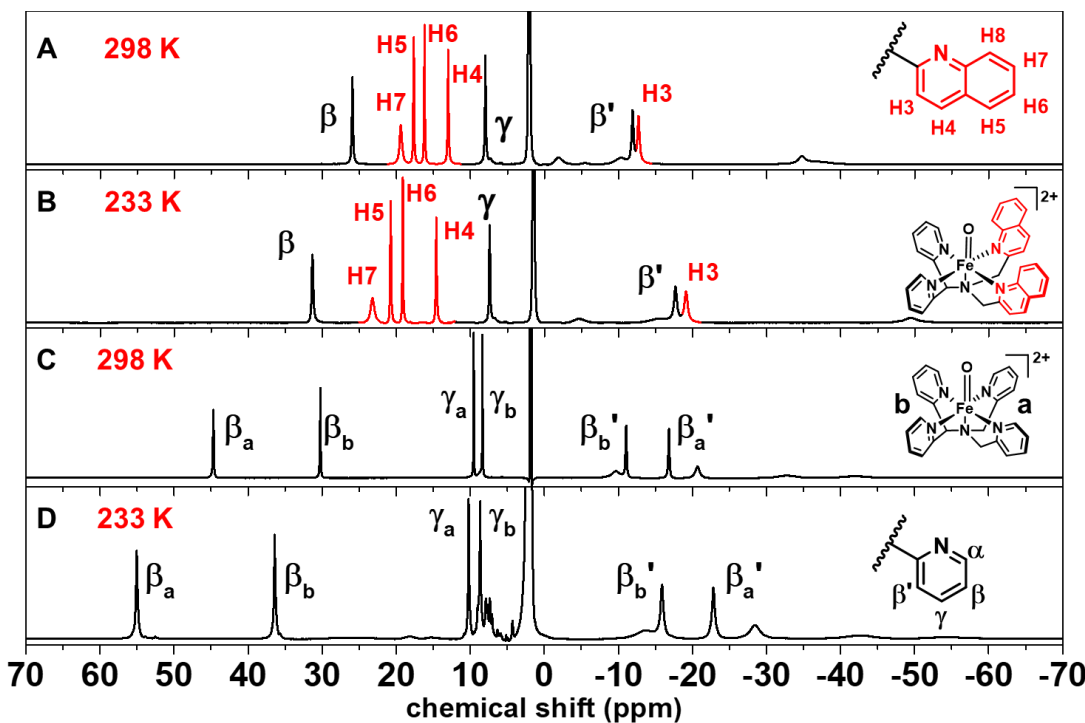


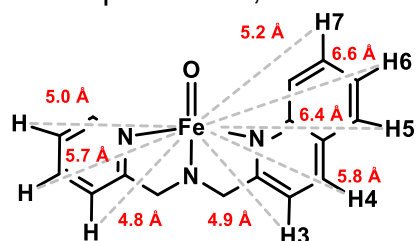
Figure S9. ${}^1\text{H}$ -NMR spectra of $[\text{Fe}^{\text{IV}}(\text{O})(\text{N}2\text{Py}2\text{Q})]^{2+}$ in acetonitrile- d_3 at 298 K (panel A) and 233 K (panel B). Quinoline peaks are highlighted in red, and denoted. ${}^1\text{H}$ -NMR spectra of $[\text{Fe}^{\text{IV}}(\text{O})(\text{N}4\text{Py})]^{2+}$ in acetonitrile- d_3 at 298 K are shown in panel C and at 233 K in panel D for comparison. See Table S5 for signal assignments in CD_3CN at 298 K.

Table S5. ${}^1\text{H}$ NMR signals of $[\text{Fe}^{\text{IV}}(\text{O})(\text{N}2\text{Py}2\text{Q})]^{2+}$ obtained in acetonitrile- d_3 at 298 K.

Legend	H3	H4	H5	H6	H7	py- γ	py- β'	py- β
δ (ppm)	-12.7	13	17.7	16.2	19.4	8	-11.9	25.9
FWHM (Hz)	140 [‡]	30	25	20	190	46	117 [‡]	58
T_1 (ms)	8	24	34	77	5	36	32	15
*d (Fe \cdots H) (\AA)	4.9	5.8	6.4	6.6	5.2	5.7	4.8	5.0

*Distances obtained from the crystal structure, with a structural representation of its cross-section shown below.²⁰

[‡]As this py- β' proton overlaps with H3, its FWHM is not very accurate.



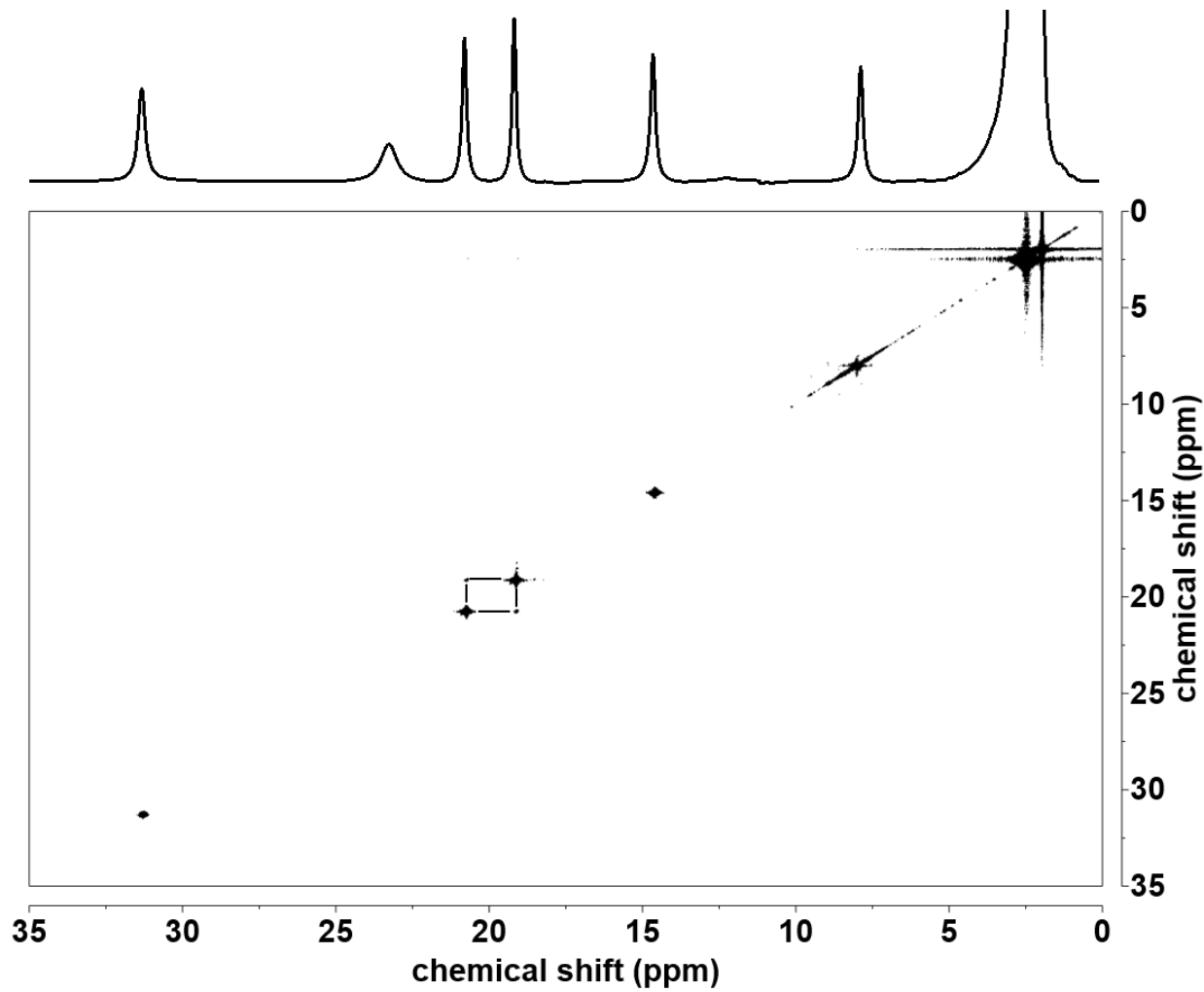


Figure S10. ${}^1\text{H}$ COSY NMR spectrum of $[\text{Fe}^{\text{IV}}(\text{O})(\text{N}_2\text{Py}_2\text{Q})]^{2+}$ in acetonitrile- d_3 at 233 K from 0 to 35 ppm. Only the peaks at 19 and 20.8 ppm are found to have relaxation properties at this temperature that allow cross-talk with each other. The lower temperature was chosen to minimize the self-decay of $[\text{Fe}^{\text{IV}}(\text{O})(\text{N}_2\text{Py}_2\text{Q})]^{2+}$ over the course of data collection time (over 12 h) on a 10-mM sample.

5) Shift patterns of S = 1 oxoiron(IV) complexes containing heterocycles

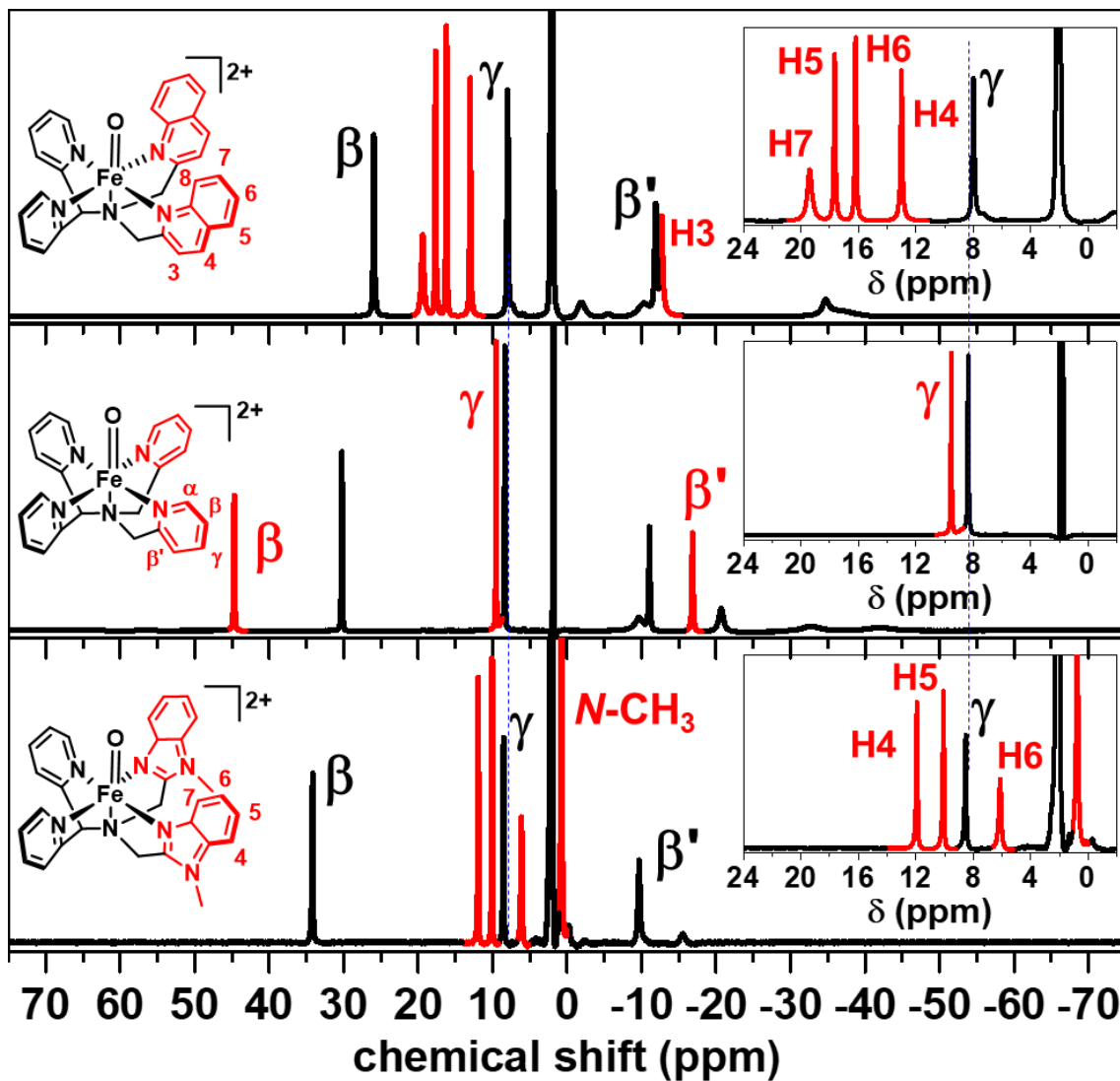


Figure S11. Stacked ^1H NMR spectra of complexes (top) $[\text{Fe}^{\text{IV}}(\text{O})(\text{N}2\text{Py}2\text{Q})]^{2+}$, (middle) $[\text{Fe}^{\text{IV}}(\text{O})(\text{N}4\text{Py})]^{2+}$ and (bottom) $[\text{Fe}^{\text{IV}}(\text{O})(\text{N}2\text{Py}2\text{B})]^{2+}$ in CD_3CN at 298 K²¹ from –75 to 75 ppm, along with assignments. The dotted lines cross through the common γ proton signal in each of the spectra.

In these oxoiron(IV) complexes, the quinoline H3 and H4 protons appear at similar chemical shifts to the pyridine γ and β' protons, respectively, indicating that these sets of protons experience similar paramagnetic effects from the S = 1 Fe^{IV} center as pyridines. This is not surprising given that a quinoline can be thought of as a pyridine having a fused phenyl ring.

H5/H6 in $[\text{Fe}^{\text{IV}}(\text{O})(\text{N}2\text{Py}2\text{Q})]^{2+}$ and H4/H5 in $[\text{Fe}^{\text{IV}}(\text{O})(\text{N}2\text{Py}2\text{B})]^{2+}$ ²¹ belong to the fused phenyl ring on the respective heterocycles and have the sharpest resonances, showing that they are likely to have relaxation properties that make them amenable to COSY spectroscopy, allowing cross-peaks to be observed in their COSY spectra obtained at

lower temperature. Because H7 in $[\text{Fe}^{\text{IV}}(\text{O})(\text{N}2\text{Py}2\text{B})]^{2+}$ and H8 in $[\text{Fe}^{\text{IV}}(\text{O})(\text{N}2\text{Py}2\text{Q})]^{2+}$ are too close to their respective iron centers, their signals are too broad to be observed. The broadest yet observable fused heterocyclic proton peaks in the NMR spectra of these ferryl complexes belong to H7 in $[\text{Fe}^{\text{IV}}(\text{O})(\text{N}2\text{Py}2\text{Q})]^{2+}$ and H6 in $[\text{Fe}^{\text{IV}}(\text{O})(\text{N}2\text{Py}2\text{B})]^{2+}$ respectively. However, H7 in $[\text{Fe}^{\text{IV}}(\text{O})(\text{N}2\text{Py}2\text{Q})]^{2+}$ is more downfield-shifted than H6 in $[\text{Fe}^{\text{IV}}(\text{O})(\text{N}2\text{Py}2\text{B})]^{2+}$. H6 in $[\text{Fe}^{\text{IV}}(\text{O})(\text{N}2\text{Py}2\text{B})]^{2+}$ is also 0.5 Å farther from the iron(IV) center than H7 in $[\text{Fe}^{\text{IV}}(\text{O})(\text{N}2\text{Py}2\text{Q})]^{2+}$, and thus its peak is less paramagnetically shifted and sharper compared with H7 in $[\text{Fe}^{\text{IV}}(\text{O})(\text{N}2\text{Py}2\text{Q})]^{2+}$. When pyridines, benzimidazoles and quinolines are viewed together, the assignments of quinoline protons in the $S = 1$ iron(IV) center are greatly facilitated by the parallels observed among pyridines, benzimidazoles and quinolines.

Table S6. ^1H NMR spectroscopic properties for complexes containing benzimidazoles or quinolines in the N4Py framework, obtained at 298 K.²¹

Legend	quinolines					benzimidazoles		
	H3	H4	H5	H6	H7	H4	H5	H6
δ (ppm)	-12.7	13	17.7	16.2	19.4	12	10	6.2
FWHM (Hz)	140	30	25	20	190	56	44	96
T_1 (ms)	8	24	34	77	5	36	59	13
**d (Fe••H) (Å)	4.9	5.8	6.4	6.6	5.2	6.3	6.8	5.7

*Distance obtained from the crystal structures, shown from cross-section.²⁰

6) ^1H -NMR spectra of oxoiron(IV) complexes and their corresponding decay products

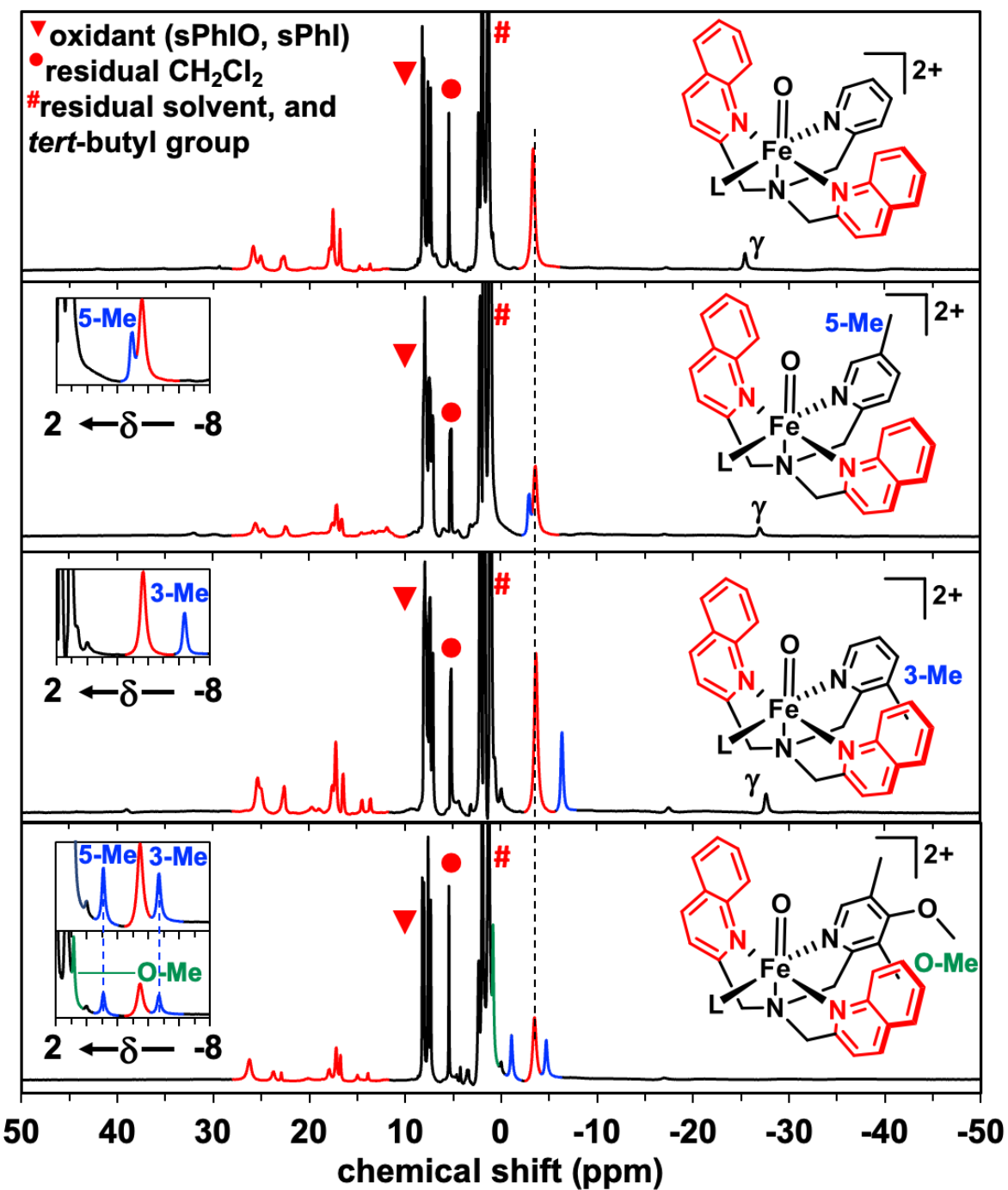


Figure S12. Stacked ^1H -NMR spectra of substituted variants of complex **2**, identifying the peaks belonging to methyl groups (insets), and other peaks between 0 to 10 ppm. Residual CH_2Cl_2 arises from CD_2Cl_2 used to dissolve the oxidant. The # indicates the *tert*-butyl group signal in the oxidant as well residual solvent signals (including CH_3CN and H_2O). Dashed lines cross a common peak through the spectra.

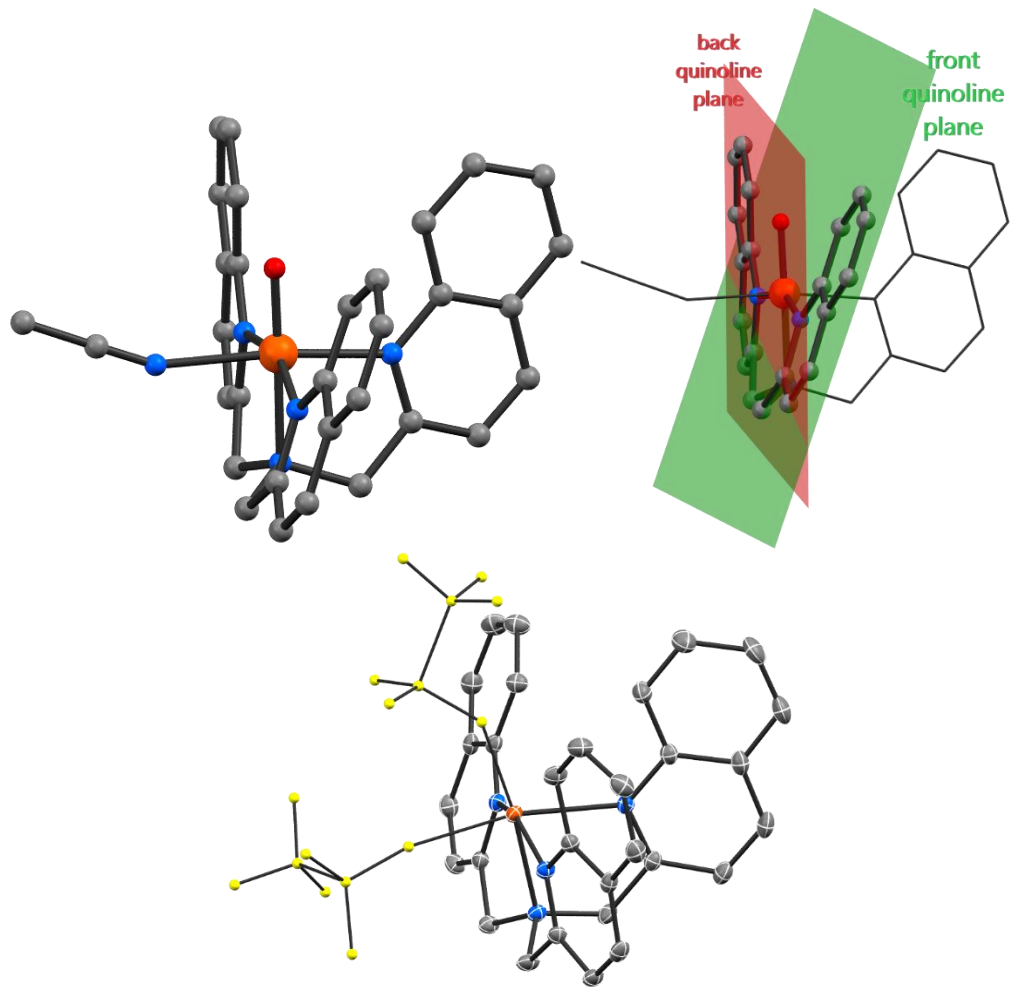


Figure S13. Evidence of C_1 symmetry in $S = 2$ complex **3** is portrayed by the DFT optimized structures of **3** (top two figures, shown as ball and stick diagrams or its combination with wireframe views of some atoms for clarity), with mean planes (green and red) formed by quinolines not aligned in the DFT structure.¹¹ It is also obvious from the iron(II) crystal structure (bottom) with thermal ellipsoids of non-hydrogen atoms at 30% (triflate atoms shown as yellow balls). The planes of the two trans quinolines are not aligned across the N–Fe–N bonds in both iron(II) and DFT-optimized iron(II) structures. N atoms = blue, iron = orange, carbon = gray, triflate ion atoms (carbon, oxygen, sulfur, fluorine) = yellow. Hydrogen atoms were hidden for clarity in all cases.

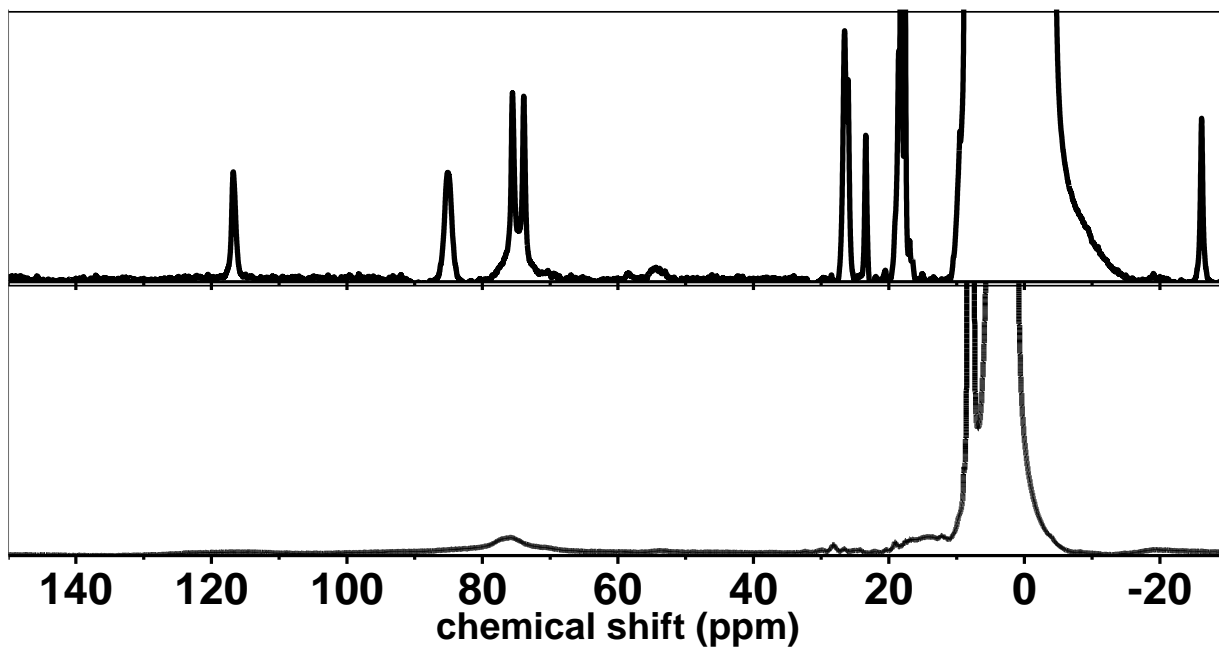


Figure S14. ¹H-NMR spectra of complex **2**, prepared by adding 2 equiv. ArIO in a 2,2,2-trifluoroethanol solution to a 4-mM solution of its iron(II) precursor in acetonitrile-*d*₃ at 233 K (top) and after its thermal decay in acetonitrile-*d*₃ at 233 K (bottom).

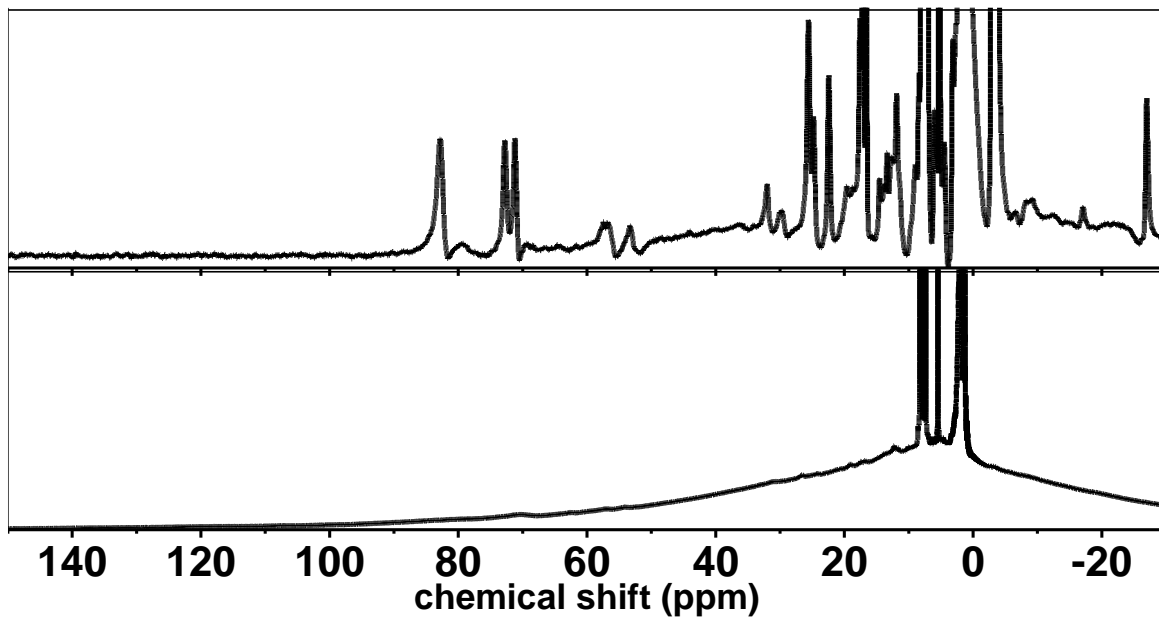


Figure S15. ¹H-NMR spectra of complex **2a** prepared by adding 2 equiv. ArIO to a 4-mM solution of its iron(II) precursor in acetonitrile-*d*₃ at 233 K (top) and after its thermal decay in acetonitrile-*d*₃ at 233 K (bottom).

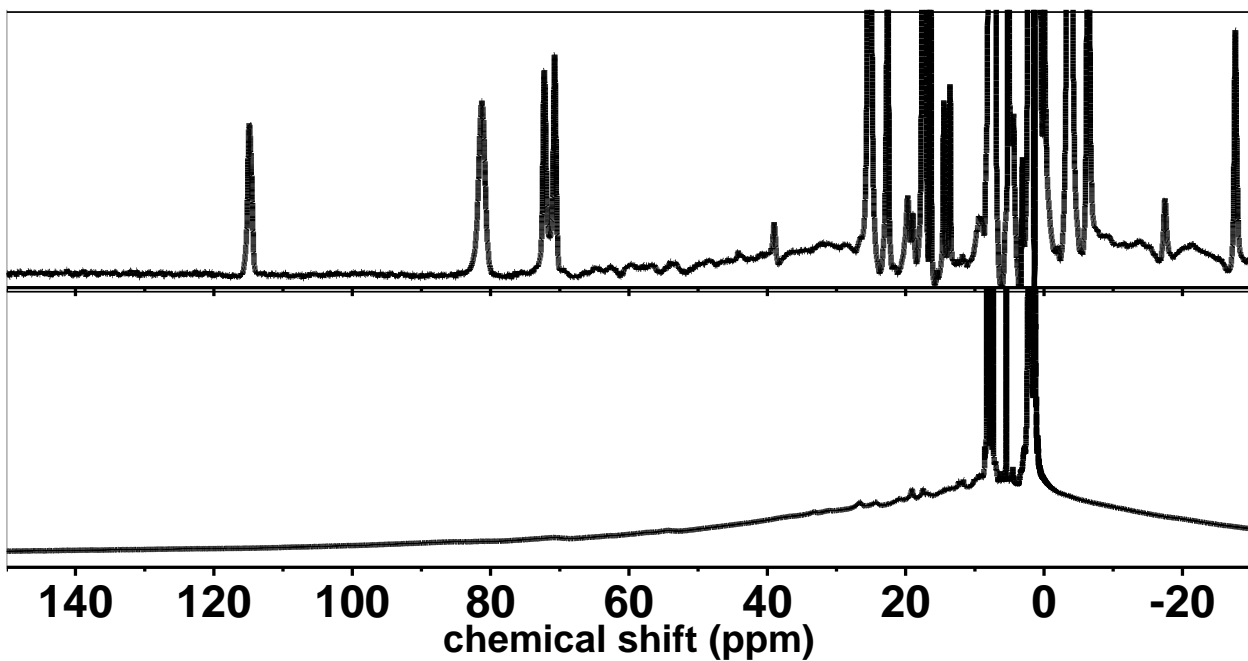


Figure S16. ¹H-NMR spectra of complex **2b**, prepared by adding 2 equiv ArIO to a 4-mM solution of its iron(II) precursor in acetonitrile-d₃ at 233 K (top) and after its thermal decay at 233 K (bottom).

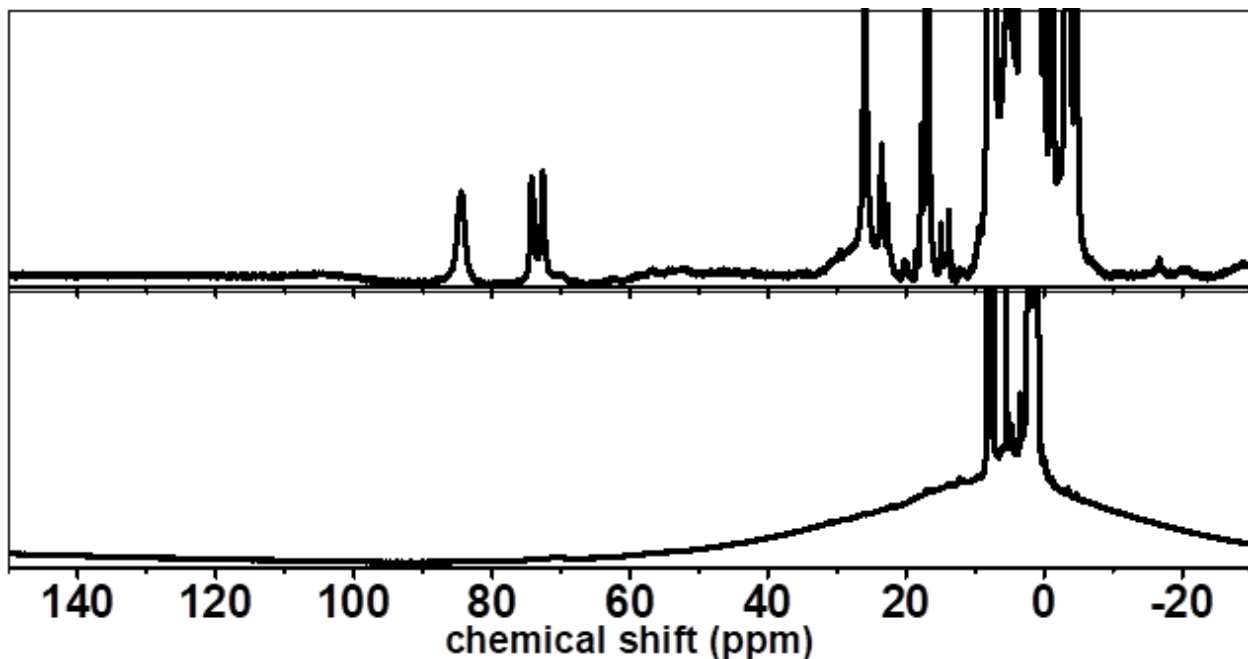


Figure S17. ¹H-NMR spectra of complex **2***, prepared by adding 2 equiv ArIO to a 4-mM solution of its iron(II) precursor in acetonitrile-d₃ at 233 K (top) and after its thermal decay (bottom).

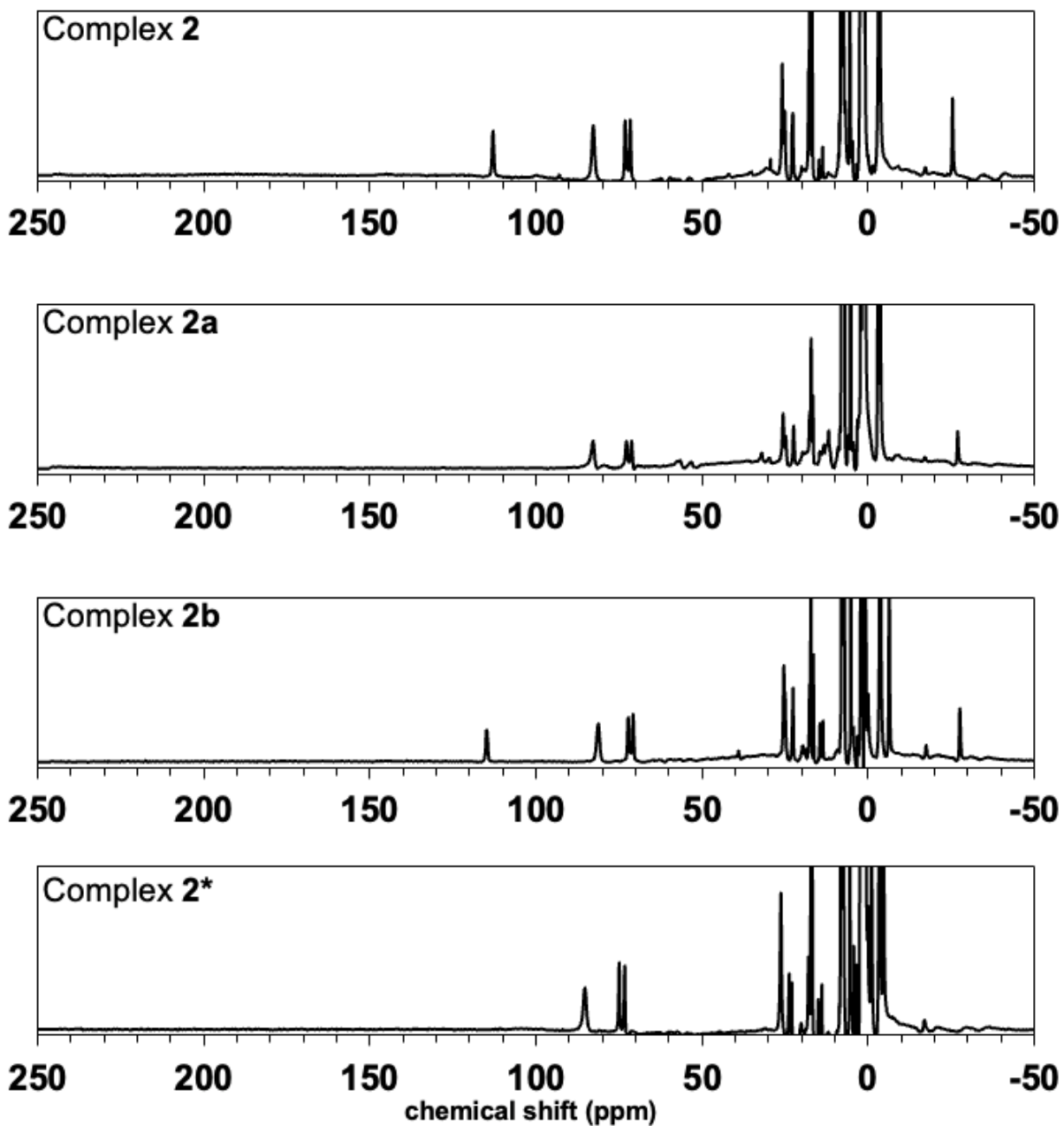


Figure S18. ¹H-NMR spectra of **2** and its variants from -50 to 250 ppm, showing that there are no observable peaks in the region past 120 ppm.

Table S7. Observed and predicted chemical shifts (in ppm) for $[\text{Fe}^{\text{IV}}(\text{O})(\text{N}2\text{Py}2\text{Q})]^{2+}$, **2** and **3** at 233 K

[Fe^{IV}(O)(N2Py2Q)]²⁺			2			3							
H	exp δ 233 K	calc δ S = 1	H	exp δ 233 K	calc δ S = 2	calc δ S = 1	H	exp δ 233 K	calc δ S = 2	calc δ S = 1			
pyridine			pyridine			pyridine			pyridine				
α	broad	-43.9 -43.9	141.9 141.9	α	not observed ^[b]	71.9	-51.7	No pyridine-H signals					
β	31	35.8 35.8	155.6 155.6	β	112	170.3	48.7	H3	quinoline				
β'	-18	-18.9 -18.9	72.7 72.7	β'	not observed ^[b]	48.1	-26.1		30 ^[a]	48.0	-21.2		
γ	7.4	10.4 10.4	-7.1 -7.1	γ	-26	-31.8	7.4		93 ^[a]	93.3	-20.7		
quinoline			quinoline			quinoline			54 ^[a]	53.0	-17.5		
H3	-19	-20.8 -20.8	72.1 72.1	H3	76, 77 or 83 ^[a]	103.5 103.5	-19.7 -19.7	H5	-5.3 ^[a]	1.7	11.9		
H4	15	15.6 15.6	1.9 1.9	H4	27, 25 or 23 ^[a]	13.6 13.6	16.2 16.2		7.2 ^[a]	8.1	13.9		
H5	21	26.0 26.0	80.2 80.2	H5	76, 77 or 83 ^[a]	89.7 89.7	21.0 21.0		-5.3 ^[a]	-29.3	11.4		
H6	19	27.3 27.3	27.8 27.8	H6	27, 25 or 23 ^[a]	28.7 28.7	30.1 30.1	H6	84 ^[a]	72.4	16.7		
H7	23	30.3 30.3	32.7 32.7	H7	27, 25 or 23 ^[a]	33.7 33.7	28.0 28.0		86 ^[a]	90.8	24.4		
H8	broad	72.8 72.8	105.5 105.5	H8	not observed ^[b]	132.4 132.4	111.5 111.5		20 ^[a]	27.1	6.7		
									23 ^[a]	33.9	34.1		
									20 ^[a]	32.9	25.5		
									18 ^[a]	26.0	18.7		
									27 ^[a]	32.7	31.6		
									26 ^[a]	25.9	25.5		
									-5.3 ^[a]	1.6	4.6		
									H8	230.6	113.8		
										270.7	166.3		
										251.6	95.6		

[a] Peaks assigned based on DFT calculations. [b] Signals not observed because they are likely to be too broad due to their proximity to the iron center

E) Mössbauer spectroscopy of oxoiron(IV) complexes

1) Generation of the ferryl complexes for NMR spectroscopic analysis

1-mM acetonitrile solutions of labeled (⁵⁷Fe) iron(II) complexes were precooled in a quartz cell at 233 K. To this stirred solution, 2 equivalents of the oxidant s-PhIO in 2,2,2-trifluoroethanol were added. The formation of the oxoiron(IV) complex was instantaneous in each case. Each sample was then transferred using cryo-cooled 9" glass pipettes into a precooled Mössbauer cup suspended on top of liquid nitrogen in a dewar.

Mössbauer spectra of a sample containing complex **1** and a sample containing the decay product of **1** were measured at 4.2 K with zero applied field (Figure S19). The decay product exhibited a quadrupole doublet with isomer shift (δ) of 0.47 mm/s and quadrupole splitting (ΔE_Q) of 1.59 mm/s, which are typical parameters from a diferric species. Such a diferric species was also observed in the sample containing **1** with almost identical Mössbauer parameters ($\delta = 0.46$ mm/s, $\Delta E_Q = 1.65$ mm/s), which represents ~ 30% of total iron in the sample. An additional quadrupole doublet was also observed in the sample containing **1**, which exhibited Mössbauer parameters $\delta = 0.05$ mm/s, $\Delta E_Q = 0.70$ mm/s, which should be assigned to **1** and represents ~ 60% of total iron. Judging by the isomer shift, **1** should still have an $S = 1$ ground spin state, although its isomer shift is 0.04 mm/s higher than that of complex **0**. The remaining spectral features belong to mononuclear ferric species as indicated by the black arrows in Figure S19.

Mössbauer spectra of a sample containing complex **2** were also measured. At 4.2 K, the spectrum exhibited two quadrupole doublets close to 1:1 ratio (Figure S19). The spectral simulation by using two quadrupole doublets led to two different solutions with equal quality of fit judging by the χ^2 value of the least square fitting. In solution I, the two quadrupole doublets have the following parameters: $\delta_1(I) = 0.03$ mm/s, $\Delta E_{Q1}(I) = 0.83$ mm/s, and $\Gamma_1(I) = 0.34$ mm/s; $\delta_2(I) = 0.53$ mm/s, $\Delta E_{Q2}(I) = 1.52$ mm/s, $\Gamma_2(I) = 0.32$ mm/s. In solution II, the parameters of the two quadrupole doublets are $\delta_1(II) = 0.10$ mm/s, $\Delta E_{Q1}(II) = 0.66$ mm/s, and $\Gamma_1(II) = 0.29$ mm/s; $\delta_2(II) = 0.44$ mm/s, $\Delta E_{Q2}(II) = 1.70$ mm/s, $\Gamma_2(II) = 0.38$ mm/s. In both solutions, site 1 should represent complex **2**, while site 2 is from the diferric decay product. Due to the similarity of the supporting ligands for **1** and **2**, it is reasonable to expect that the Mössbauer parameters of the diferric decay product of **2** should be similar with those of the decay product of **1**. Based on this, solution II should be the correct solution. However, since both solutions produce a similar quality of fit to the experimental data, we sought additional experimental support for solution II. Variable field and temperature Mössbauer analysis was then carried out. In Figure S20, the spectral features belonging to the diamagnetic ($S = 0$) diferric species are indicated by black arrows. The magnitude of magnetic splitting of an $S = 0$ species depends on magnitude of quadrupole splittings and the magnitude of externally applied magnetic field. In solutions I and II described above, the quadrupole splittings of the diferric species are very different. Thus, the spectral features of the diamagnetic diferric species in the 7-T spectrum should provide strong evidence to distinguish the two spectral simulation solutions. Indeed, the use of $\Delta E_Q = 1.70$ mm/s can nicely reproduce the spectral features of the diferric species in the 7-T spectrum, while the use of $\Delta E_Q = 1.52$ mm/s cannot.

Therefore, solution II is a better solution to describe the spectra measured on the sample containing **2** with the quadrupole doublet having $\delta_1(\text{II}) = 0.10 \text{ mm/s}$, $\Delta E_{Q1}(\text{II}) = 0.66 \text{ mm/s}$ to represent **2**. In addition, by using the variable field and temperature Mössbauer data, we determined that **2** still retained an $S = 1$ ground spin state with a large and positive D ($D \sim 35 \text{ cm}^{-1}$) and an axial ^{57}Fe hyperfine tensor ($A_x = A_y = -23 \text{ T}$) (**Figure S21**). Interestingly, the isomer shifts of complexes **0**, **1**, and **2** exhibit a clear pattern, where an increase in the number of quinoline donors on the supporting ligand leads to higher isomer shift. This is consistent with the correlation between isomer shift and iron-ligand bond length initially identified by Neese,²² namely longer iron-ligand bonds give rise to higher isomer shift. Therefore, the current isomer shift trend suggests that in going from complex **0** to **2**, the average iron-ligand bond length increases due to an increase in the number of quinoline donors.

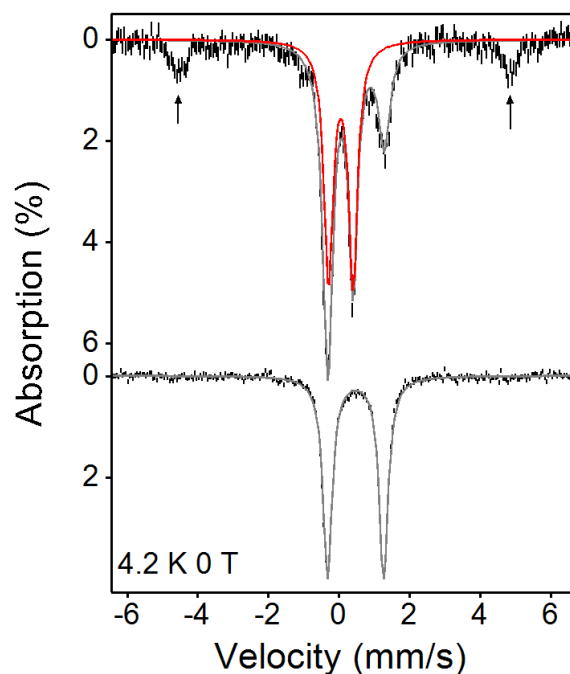


Figure S19. Zero field Mössbauer spectra of a sample containing complex **1** (top) and a sample containing the diferric decay product of **1** (bottom) measured at 4.2 K. The experimental data are shown as vertical black bars, the overall simulations of the spectra are shown as the grey solid lines, and the spectral simulation of **1** is indicated as the red solid line. The spectral features indicated by the black arrows belong to mononuclear high-spin ferric species. The simulation parameters are listed in **Table S8**.

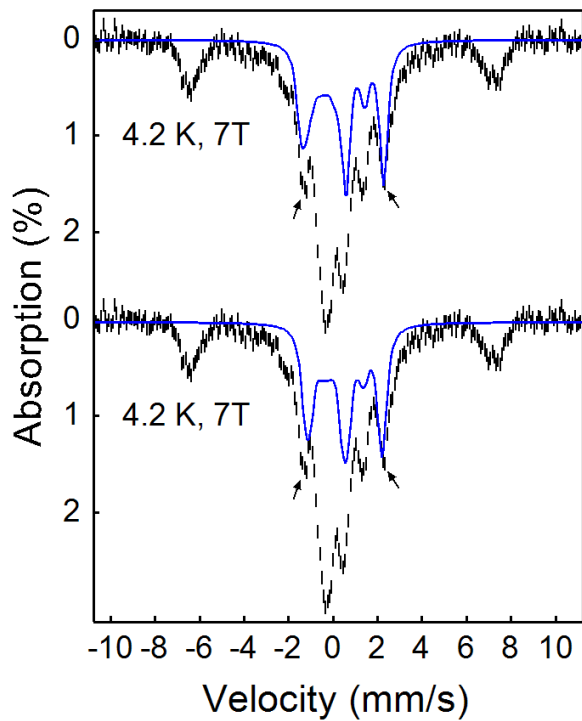


Figure S20. 4.2 K and 7 T Mössbauer spectra of a sample containing **2**. The black arrows indicate the spectral features belonging to the diamagnetic diferric decay product. The experimental data are shown as the vertical black bars and the simulations of the diamagnetic diferric decay product are shown in blue, which are generated by the simulation parameters from solution II (top) and from solution I (bottom). It is clearly shown that the simulated spectrum generated by the parameters of solution I does not match the diferric spectral feature well, while the parameters of solution II do.

Table S8. Mössbauer simulation parameters of various species.^[a]

Temp (K)	Species	Simulation Solution	$\Delta^{[a]}$ (mm/s)	ΔE_Q (mm/s)	Γ (mm/s)	%A
4.2	1	-	0.05	0.70	0.34	48
	Di-ferric decay product of 1	-	0.46	1.65	0.32	45
4.2	Di-ferric species ^[b]	-	0.47	1.59	0.33	100
4.2	2	Solution I	0.03	0.83	0.34	48
		Solution II	0.10	0.66	0.29	45
4.2	Di-ferric decay product of 2	Solution I	0.53	1.52	0.32	45
		Solution II	0.45	1.70	0.38	50
150	2	Solution II	0.08	0.63	0.36	46
	Di-ferric decay product of 2		0.42	1.76	0.50	53

^[a]The change in isomer shifts at different temperatures originates from the second order Doppler effect on isomer shift due to the difference on the source temperature and the sample temperature.

^[b]The di-ferric species obtained from the fully decay of complex **1**.

5. DFT calculations for oxoiron(IV) complexes

We optimized the structures of complexes $[\text{Fe}^{\text{IV}}(\text{O})(\text{N}2\text{Py}2\text{Q})]^{2+}$, **2**, and **3** in Gaussian 16 (Rev. B01)²³ in both the $S = 1$ and the $S = 2$ states with modified B3LYP²⁴⁻²⁶ (labeled as B3LYP* in the following) functionals (lop(3/76=1000001500) lop(3/77=0720008000) lop(3/78=0810010000)), a 6-31G(d,p') basis set and a built-in acetonitrile solvation model (scrf=(solvent=acetonitrile)).²⁷ The empirical dispersion using the D3 version of Grimme's dispersion with the original D3 damping function was also included in the geometry optimization.²⁸ To obtain a more precise result, we ran the optimization with a small step size (opt=maxstep=10), while the default value of maxstep was 30. For complex **2**, a C_s symmetry was enforced during the geometry optimization. Then we performed $^1\text{H-NMR}$ shift calculations by using the same functional but with a Dunning correlation-consistency basis set cc-pVTZ by following the protocols described by Bagno and coworkers.²⁹⁻³²

The calculated $^1\text{H-NMR}$ shifts were determined by the following formula:^{33, 34}

$$\sigma = \sigma_{\text{ref}} - (\sigma_{\text{orb}} + \sigma_{\text{FC}} + \sigma_{\text{PC}})$$

where $\sigma_{\text{ref}} = 31.03$ ppm for TMS was obtained at the same theoretical level as those for the Fe(IV) complexes included in this study. σ_{orb} is the orbital contribution to the proton, which is equivalent to the shielding for diamagnetic systems. The Fermi contact term, σ_{FC} , which originates from the scalar interaction between magnetic field from unpaired electrons and the magnetic momentum of target proton, dominates the paramagnetic component in the $^1\text{H-NMR}$ shift arising from the paramagnetic center. The Fermi contact term can be calculated from Fermi's hyperfine interaction parameters as the following:

$$\sigma_{\text{FC}} = \frac{2\pi}{\gamma_I} g_{\text{iso}} \mu_B A \frac{S(S+1)}{3kT}$$

in which γ_I is the magnetogyric ratio of the nucleus I and g_{iso} is the isotropic g factor of the spin system, μ_B is the Bohr magneton and A is the Fermi hyperfine interaction parameter. For $[\text{Fe}^{\text{IV}}(\text{O})(\text{N}2\text{Py}2\text{Q})]^{2+}$, the g values have been determined by high field EPR measurements,¹² therefore for this complex we used the experimentally determined g values to determine g_{iso} , which is 2.05. We then used this value for all the $S = 1$ state NMR calculations. For the $S = 2$ complex **3**, no experimentally determined g values are available. However, the literature reported g values for two other $S = 2$ oxoiron(IV) complexes, $[\text{Fe}^{\text{IV}}(\text{O})\text{H}_3\text{buea}]^{-4}$ and $[\text{Fe}^{\text{IV}}(\text{O})(\text{tpa}^{\text{Ph}})]^{-2}$ are all close to 2, therefore, for all the $S = 2$ state NMR calculations, g_{iso} is fixed at 2. The contribution from pseudo-contact term σ_{PC} , can be approximated by the theory developed by Hrobárik et al.³⁵ Usually it is small and can be ignored compared with σ_{FC} . In this work we estimate the $^1\text{H-NMR}$ shift only by the orbital term and Fermi-contact term. All calculations were done at 233 K, the same temperature at which most of the $^1\text{H-NMR}$ measurements were performed in this work.

Table S9. Selected bond lengths of the DFT optimized structures for complexes **1 - 3**.

Spin State	Complex	Bond Length (Å)			
		Fe–N _{eq} ^[a]	Fe–N _{ax} ^[b]	Fe=O	Fe–N _{avg} ^[c]
S = 1	1	1.974, 1.997, 2.057, 1.975	2.103	1.648	2.021
	2	1.971, 1.978, 2.069, 2.069	2.089	1.647	2.035
	3	2.075, 2.075, 2.064, 1.988	2.088	1.646	2.058
S = 2	1	2.095, 2.145, 2.118, 2.237	2.132	1.635	2.145
	2	2.199, 2.199, 2.088, 2.194	2.120	1.631	2.160
	3	2.111, 2.166, 2.196, 2.206	2.090	1.637	2.154

[a] The Fe–N bond lengths of the ligands in the equatorial plane that is perpendicular to the Fe=O axis.

[b] The Fe–N bond length of the ligand trans to the Fe=O moiety.

[c] The averaged Fe–N bond lengths.

Table S10. Calculated & experimental ¹H NMR parameters for S = 1 [Fe^{IV}(O)(N2Py2Q)]²⁺ at 233 K in CD₃CN.

protons	σ^{orb}	A (MHz)	σ^{FC}	$\sigma^{\text{FC}}(\text{total})$	$\delta_{\text{calculated}}$	$\delta_{\text{experimental}}$
py						
β	23.1722	0.30067	-27.917657	-4.7454575	35.8254575	31
	23.1722	0.30067	-27.917657	-4.7454575	35.8254575	
γ	22.6214	0.02067	-1.9192403	20.7021597	10.3778403	7.4
	22.6214	0.02067	-1.9192403	20.7021597	10.3778403	
β'	23.0058	-0.29069	26.9909996	49.9967996	-18.9168	-18
	23.0058	-0.29069	26.9909996	49.9967996	-18.9168	
α	21.3535	-0.57765	53.6356632	74.9891632	-43.909163	unassigned
	21.3535	-0.57765	53.6356632	74.9891632	-43.909163	
quin						
H3	23.7747	-0.30366	28.1952834	51.9699834	-20.889983	-19
	23.7747	-0.30366	28.1952834	51.9699834	-20.889983	
H4	22.7138	0.07752	-7.1978475	15.5159525	15.5640475	14.6
	22.7138	0.07752	-7.1978475	15.5159525	15.5640475	
H5	22.9946	0.19355	-17.971406	5.02319412	26.0568059	20.7
	22.9946	0.19355	-17.971406	5.02319412	26.0568059	
H6	22.9066	0.20636	-19.160833	3.74576654	27.3342335	19.1
	22.9066	0.20636	-19.160833	3.74576654	27.3342335	
H7	22.5244	0.23422	-21.747676	0.77672403	30.303276	23.2
	22.5244	0.23422	-21.747676	0.77672403	30.303276	
H8	19.4063	0.65852	-61.144563	-41.738263	72.8182632	too broad
	19.4063	0.65853	-61.145492	-41.739192	72.8191917	

Table S11. Calculated & experimental ^1H NMR parameters for $S = 2$ $[\text{Fe}^{\text{IV}}(\text{O})(\text{N}2\text{Py}2\text{Q})]^{2+}$ at 233 K in CD_3CN .

protons	σ^{orb}	A (MHz)	σ^{FC}	σ^{FC} (total)	$\delta_{\text{calculated}}$	$\delta_{\text{experimental}}$
py						
β	22.9674	0.54474	-147.53501	-124.56761	155.647614	31
	22.9675	0.5448	-147.55126	-124.58376	155.663764	
γ	22.5439	-0.05763	15.6082587	38.1521587	-7.0721587	7.4
	22.544	-0.05758	15.5947169	38.1387169	-7.0587169	
β'	23.0896	0.23905	-64.743263	-41.653663	72.733663	-18
	23.0896	0.23914	-64.767638	-41.678038	72.7580382	
α	21.2823	0.48771	-132.08926	-110.80696	141.886957	unassigned
	21.2825	0.48797	-132.15967	-110.87717	141.957174	
quin						
H3	23.9741	0.23982	-64.951806	-40.977706	72.0577065	-19
	23.9743	0.23976	-64.935556	-40.961256	72.0412563	
H4	22.6339	-0.0243	6.58130638	29.2152064	1.86479362	14.6
	22.634	-0.0243	6.58130638	29.2153064	1.86469362	
H5	22.9883	0.26613	-72.077493	-49.089193	80.1691925	20.7
	22.9883	0.26612	-72.074784	-49.086484	80.1664842	
H6	22.9113	0.07232	-19.586834	3.32446553	27.7555345	19.1
	22.9112	0.07234	-19.592251	3.31894881	27.7610512	
H7	22.6867	0.0897	-24.293958	-1.6072581	32.6872581	23.2
	22.6865	0.0897	-24.293958	-1.6074581	32.6874581	
H8	20.6385	0.35109	-95.08769	-74.44919	105.52919	too broad
	20.6382	0.35114	-95.101231	-74.463031	105.543031	

Table S12. Calculated & experimental ^1H NMR parameters for a C_s -symmetric structure of $S = 1$ complex **2** ($[\text{Fe}^{IV}(\text{O})(\text{BQPA})(\text{CD}_3\text{CN})]^{2+}$) at 233 K in CD_3CN .

protons	σ^{orb}	A (MHz)	σ^{FC}	$\sigma^{\text{FC}}(\text{total})$	$\delta_{\text{calculated}}$	$\delta_{\text{experimental}}$
py						
β	23.5444	0.45571	-42.24478441	-18.70038441	49.7803844	118
γ	23.2122	-0.0047	0.435694821	23.64789482	7.43210518	-26
β'	23.8816	-0.36858	34.16774405	58.04934405	-26.969344	unassigned
α	20.7705	-0.68677	63.66428341	84.43478341	-53.354783	unassigned
quin						
H3	23.3565	-0.30443	28.22097325	51.57747325	-20.497473	76, 77, or 83
	23.3569	-0.30417	28.19687098	51.55377098	-20.473771	
H4	22.3234	0.08221	-7.620951322	14.70244868	16.3775513	27, 25, or 23
	22.3238	0.08256	-7.653396681	14.67040332	16.4095967	
H5	22.6686	0.13958	-12.93920917	9.729390835	21.3506092	76, 77, or 83
	22.6688	0.14033	-13.00873493	9.660065066	21.4199349	
H6	22.6918	0.2397	-22.22043586	0.471364143	30.6086359	27, 25, or 23
	22.6919	0.24017	-22.26400534	0.427894661	30.6521053	
H7	22.4242	0.21465	-19.89827516	2.525924837	28.5540752	27, 25, or 23
	22.4242	0.21532	-19.96038485	2.46381515	28.6161849	
H8	19.5847	1.1068	-102.6014952	-83.01679523	114.096795	Not observed
	19.5826	1.10902	-102.8072915	-83.2246915	114.304692	

Table S13. Calculated & experimental ^1H NMR parameters for a C_s -symmetric structure of $S = 2$ complex **2** ($[\text{Fe}^{IV}(\text{O})(\text{BQPA})(\text{CD}_3\text{CN})]^{2+}$) at 233 K in CD_3CN .

protons	σ^{orb}	A (MHz)	σ^{FC}	$\sigma^{\text{FC}}(\text{total})$	$\delta_{\text{calculated}}$	$\delta_{\text{experimental}}$
py						
β	23.4355	0.6007	-162.6909772	-139.2554772	170.335477	112
γ	23.192	-0.14672	39.73700711	62.92900711	-31.849007	-26
β'	24.0656	0.15177	-41.10472716	-17.03912716	48.1191272	unassigned
α	21.1695	0.22871	-61.94282235	-40.77332235	71.8533224	unassigned
quin						
H3	23.514	0.35417	-95.92186346	-72.40786346	103.487863	76, 77, or 83
	23.514	0.35417	-95.92186346	-72.40786346	103.487863	
H4	22.1737	0.01727	-4.677331739	17.49636826	13.5836317	27, 25, or 23
	22.1737	0.01727	-4.677331739	17.49636826	13.5836317	
H5	22.598	0.29986	-81.21277911	-58.61477911	89.6947791	76, 77, or 83
	22.598	0.29986	-81.21277911	-58.61477911	89.6947791	
H6	22.6424	0.07484	-20.26934032	2.373059679	28.7069403	27, 25, or 23
	22.6424	0.07484	-20.26934032	2.373059679	28.7069403	
H7	22.5098	0.09262	-25.08479824	-2.574998244	33.6549982	27, 25, or 23
	22.5098	0.09262	-25.08479824	-2.574998244	33.6549982	
H8	20.7867	0.45094	-122.1306297	-101.3439297	132.42393	Not observed
	20.7867	0.45094	-122.1306297	-101.3439297	132.42393	

Table S14. Calculated & experimental ^1H NMR parameters for $S = 1$ complex **3** ($[\text{Fe}^{IV}(\text{O})(\text{TQA})(\text{CD}_3\text{CN})]^{2+}$) at 233 K in CD_3CN .

protons	σ^{orb}	A (MHz)	σ^{FC}	$\sigma^{\text{FC}}(\text{total})$	$\delta_{\text{calculated}}$	$\delta_{\text{experimental}}$
quin						
H3	23.773	-0.31608	29.13924048	52.91224048	-21.83224	93
H4	22.8036	0.0398	-3.66914	19.13446	11.94554	7.2
H5	23.0412	0.09571	-8.823451994	14.21774801	16.862252	86
H6	22.9618	0.28811	-26.56070164	-3.598901641	34.6789016	20
H7	22.5711	0.25625	-23.62354585	-1.052445852	32.1324459	27
H8	19.2029	1.12873	-104.0569948	-84.85409477	115.934095	unassigned
quin						
H3	23.3379	-0.28014	25.82595175	49.16385175	-18.083852	54
H4	22.2139	0.02825	-2.604351884	19.60954812	11.4704519	-5.3
H5	22.6906	-0.01839	1.695363935	24.38596393	6.69403607	20
H6	22.8202	0.1156	-10.6571001	12.1630999	18.9169001	18
H7	22.9041	-0.03952	3.643326954	26.54742695	4.53257305	-5.3
H8	21.2133	1.73327	-159.7892032	-138.5759032	169.655903	unassigned
quin						
H3	23.4572	-0.31368	28.91798581	52.37518581	-21.295186	30
H4	22.6316	0.06053	-5.580227241	17.05137276	14.0286272	-5.3
H5	23.0158	0.1814	-16.72316573	6.292634273	24.7873657	84
H6	22.9163	0.19186	-17.68746735	5.228832655	25.8511673	23
H7	22.5065	0.19698	-18.15947731	4.347022685	26.7329773	26
H8	19.525	0.93092	-85.82100021	-66.29600021	97.3760002	unassigned

Table S15. Calculated & experimental ^1H NMR parameters for $S = 2$ complex **3** ($[\text{Fe}^{IV}(\text{O})(\text{TQA})(\text{CD}_3\text{CN})]^{2+}$) at 233 K in CD_3CN .

protons	σ^{orb}	A (MHz)	σ^{FC}	$\sigma^{\text{FC}}(\text{total})$	$\delta_{\text{calculated}}$	$\delta_{\text{experimental}}$
quin						
H3	23.9975	0.3184	-86.23407213	-62.23657213	93.3165721	93
H4	22.6705	-0.00103	0.278960723	22.94946072	8.13053928	7.2
H5	23.009	0.30535	-82.69966685	-59.69066685	90.7706669	86
H6	22.9383	0.09123	-24.70833669	-1.770036685	32.8500367	20
H7	22.7087	0.10174	-27.55481941	-4.846119405	35.9261194	27
H8	20.6384	0.51294	-138.9224402	-118.2840402	149.36404	unassigned
quin						
H3	23.3847	0.16738	-45.33247171	-21.94777171	53.0277717	54
H4	22.0083	-0.14165	38.36387034	60.37217034	-29.29217	-5.3
H5	22.5243	0.06833	-18.50620022	4.018099784	27.0619002	20
H6	22.648	0.06492	-17.58265064	5.065349363	26.0146506	18
H7	22.6538	-0.02524	6.835891899	29.4896919	1.5903081	-5.3
H8	21.1068	0.81684	-221.2293954	-200.1225954	231.202595	unassigned
quin						
H3	23.7614	0.15008	-40.6470149	-16.8856149	47.9656149	30
H4	22.5527	-0.02525	6.838600255	29.39130026	1.68869974	-5.3
H5	22.9878	0.2373	-64.26930062	-41.28150062	72.3615006	84
H6	22.9429	0.09505	-25.74292888	-2.800028882	33.8800289	23
H7	22.7485	0.09014	-24.41312582	-1.664625823	32.7446258	26
H8	20.5867	0.49763	-134.7759463	-114.1892463	145.269246	unassigned

Table S16. The calculated free energy difference between $\text{Fe}^{(IV)}=\text{O}$ complexes and their corresponding one-electron reduced complexes ^a

	0	1	2 (S = 2)	2 (S = 1)	3
$\Delta G(\text{Fe}^{III}/\text{Fe}^{IV})$ (Kcal/mol)	-118.506	-121.372	-125.003	-125.344	-127.3
$\Delta\Delta G(\text{Fe}^{III}/\text{Fe}^{IV})$ (Kcal/mol) ^b	0	-2.865	-6.497	-6.839	-8.769
ΔE (mV) ^c	0	124	281	297	380

^a $\Delta G(\text{Fe}^{III}/\text{Fe}^{IV}) = G(\text{Fe}^{III}) - G(\text{Fe}^{IV})$

^b $\Delta\Delta G(\text{Fe}^{III}/\text{Fe}^{IV})$ is the relative free energy differences between complexes 1, 2 ($S = 2$), 2 ($S = 1$) and 3 to complex 0 by setting $\Delta G(\text{Fe}^{III}/\text{Fe}^{IV})$ of complex 0 as the reference (setting the value to be zero).

^c ΔE is the relative reduction potential differences between complexes 1, 2 ($S = 2$), 2 ($S = 1$) and 3 to complex 0 by setting the reduction potential of complex 0 as the reference.

6. DFT Coordinates

Coordinates of S = 1 [Fe^{IV}(O)(N2Py2Q)]²⁺:

Fe	0.59070800	0.00000000	-0.39261300	N	2.18741100	1.43799500	-0.65965800	C	4.04658400	-1.35092400	-0.24316700
O	0.19157000	-0.00000300	-1.98936600	C	3.41849200	3.32943600	-1.50525700	C	5.19885500	-0.99556200	-1.02387700
N	1.41123200	0.00000600	1.51900900	H	3.49550500	4.14708100	-2.23615000	C	5.04775800	-0.39819100	-2.27251300
C	2.88961000	0.00000000	1.12293300	C	2.31328300	2.45541000	-1.54757000	C	3.73611500	-0.14515000	-2.78828200
H	3.57317200	0.00000200	1.99483100	H	1.50599000	2.54842700	-2.28906400	C	2.59453400	-0.46686200	-2.05271900
N	-0.68080900	1.40627400	0.40206400	C	3.14425800	-1.23935200	0.29856400	C	2.71975500	-1.06304600	-0.75763800
C	3.06593600	1.23169500	0.22280400	H	4.27189200	-2.06703700	0.40588200	H	-2.30217000	-2.19337400	2.82793800
N	-0.68081200	-1.40626700	0.40207000	C	5.27669100	-3.80338800	-0.45852000	H	-6.33456400	-0.34454300	0.83610700
C	4.16132600	2.10675700	0.21268000	C	3.41817100	-3.32981400	-1.50471400	H	-6.64693000	1.58560600	-0.73383100
N	2.01052100	1.37895200	-0.63757600	C	3.49510600	-4.14758600	-2.23547400	H	5.64510300	3.35807200	-2.21450300
C	3.06448400	3.31315500	-1.60680700	C	2.31305700	-2.45567600	-1.54718100	H	-3.14351300	3.48434100	-2.500083400
H	4.99006900	1.96154300	0.91900300	H	1.50575800	-2.54873100	-2.28866400	C	-1.64821400	1.83310800	-1.38316500
N	2.01052100	-1.37895900	-0.63756700	C	0.88172500	1.25219600	2.15674600	H	-0.17827400	-0.66720900	3.66865600
C	4.15603000	3.16848000	-0.72414700	H	1.60623300	2.06783300	1.95634900	C	-1.52944400	0.15193500	2.83105700
H	4.99804800	3.87624200	-0.75839800	H	0.87389600	1.08568400	3.25256500	H	1.02668300	1.40432800	4.21765700
N	2.01052700	1.37895200	-0.63757600	C	-0.48680000	1.69997300	1.65055500	C	2.37785800	3.38257800	3.40153400
C	3.06448400	3.31315500	-1.60680700	C	-1.37310600	2.39053300	2.52626400	H	3.14956300	4.80189400	1.48672900
H	3.03047700	4.12587600	-2.34635000	H	-1.08641200	2.54101100	3.57713000	H	3.19700200	5.27082900	-0.98585400
C	1.99878100	2.39408100	-1.53736900	C	-2.59000200	2.84911900	2.02977900	H	1.93235700	3.76884700	-2.56898100
H	1.12171600	2.43819900	-2.19804400	H	-3.30419600	3.37202900	2.68607500	H	0.64464100	1.81241000	-1.71419600
C	3.06593000	-1.23170200	0.22281300	C	-2.92033300	2.64040000	0.65449900	H	0.11278300	-3.38965200	1.40865800
C	4.16131500	-2.10677000	0.21128400	C	-4.15872500	3.09951300	0.08682200	H	0.61943100	-2.64810400	2.96185900
H	4.99005900	-1.96155500	0.91901800	H	-4.87433900	3.62504800	0.73949200	H	3.06466800	-2.84642300	2.70961400
C	4.15601400	-3.16849900	-0.72412400	C	-4.43773900	2.88542900	-1.26082800	H	5.16010500	-2.20583800	1.44081600
H	4.99802900	-3.87626600	-0.75837000	H	-5.38632100	3.23873400	-1.69439500	C	6.19854000	-1.21350100	-0.61488600
C	3.06446700	-3.31317500	-1.60678300	C	-3.48462200	2.21072300	-2.08988200	H	5.93232300	-0.12854400	-2.87025900
H	3.03045700	-4.12590100	-2.34632100	H	-3.70810800	2.05653400	-3.15748300	H	3.62400900	0.31038600	-3.78494800
C	1.99876900	-2.39409500	-1.53735200	C	-2.27589300	1.74495600	-1.57031300	H	1.59146300	-0.27996700	-2.45558800
H	1.12170500	-2.43821300	-2.19802700	H	-1.54376400	1.23483900	-2.20949200	C	-1.15024900	-3.57388300	-1.65077400
C	0.96004400	1.25005700	2.23426700	C	-1.96936800	1.93945300	-0.18563100	C	-1.40952100	-4.78272700	-2.44282300
H	1.70284600	2.05645200	2.06202200	C	0.88157900	-1.25172300	2.15694900	H	-2.50356000	-4.90478800	-2.58036100
H	0.91644700	1.08146800	3.32875400	H	0.87358500	-1.08496900	3.25273000	H	-0.92020400	-4.68618300	-3.43370300
C	-0.38667900	1.71575500	1.68915500	C	1.60610100	-2.06742300	1.95685100	H	-1.00120300	-5.66692900	-1.91162800
C	-1.24020400	2.49181800	2.52402200	C	-0.48688400	-1.69960500	1.65067800				
H	-0.93774800	2.68968300	3.56258600	C	-1.37322600	-2.39010300	2.52640300				
C	-2.44122400	2.96511100	2.01069800	H	-1.08660900	-2.54043200	3.57731200				
H	-3.13335700	3.54902500	2.63830100	C	-2.59005100	-2.84882800	2.02987700				
C	-2.78069000	2.69728500	0.64849400	H	-3.30426700	-3.37169700	2.68618100				
C	-3.99764200	3.18968000	0.06613700	C	-2.91977000	-2.64031600	0.65454000				
H	-4.68357500	3.77200400	0.70216100	C	-4.15858700	-3.09959500	0.08681800				
C	-4.29219100	2.94423000	-1.27209500	H	-4.87422300	-3.62508500	0.73949900				
H	-5.22464900	3.32561900	-1.71658400	C	-4.43749200	-2.88572800	-1.26088900				
C	-3.36778500	2.20517200	-2.07562300	H	-5.38601100	-3.23916200	-1.69449200				
H	-3.59148700	2.03143100	-3.14021300	C	-3.48434400	-2.21108200	-2.08995400				
C	-2.18191400	1.70030200	-1.53954500	H	-3.70773900	-2.05706900	-3.15760000				
H	-1.47273100	1.15011300	-2.16854800	C	-2.27569600	-1.74515400	-1.57034200				
C	-1.86226900	1.91592400	-0.16093700	H	-1.54354300	-1.23508300	-2.20953100				
C	0.96003700	-1.25005600	2.23427600	C	-1.96928500	-1.93942200	-0.18560300				
H	0.91643900	-1.08144000	3.32876200								
H	1.70283400	-2.05643800	2.06203800								
C	-0.38667900	-1.71573400	1.68916700								
C	-1.24022000	-2.49178400	2.52403800								
H	-0.93777000	-2.68963800	3.56260600								
C	-2.44123800	-2.96508000	2.01071400								
H	-3.13337600	-3.54898400	2.63832100								
C	-2.78069500	-2.69727200	0.64850500								
C	-3.99764500	-3.18967300	0.06614600								
H	-4.68358300	-3.77119800	0.70217300								
C	-4.29218400	-2.94424200	-1.27209100								
H	-5.22463900	-3.32563600	-1.71658100								
C	-3.36777000	-2.20519700	-2.07562400								
H	-3.59146400	-2.03147200	-3.14021800								
C	-2.18190300	-1.70032100	-1.53954500								
H	-1.47271500	-1.15014100	-2.16855100								
C	-1.86226800	-1.91592300	-0.16093200								

Coordinates of S = 2 [Fe^{IV}(O)(N2Py2Q)]²⁺:

Coordinates of S = 2 [Fe^{IV}(O)(TQA)NCCH₃]²⁺:

Fe	-0.42731900	-0.61620600	-0.23624400	N	-2.45475400	-0.20801500	0.18574600	C	0.31091200	-0.68873900	0.21512200
N	-2.45475400	-0.20801500	0.18574600	H	0.40895200	1.08711900	0.86946500	N	2.31794400	-0.38255600	-0.10375000
C	-2.44123800	-2.96508000	2.01071400	H	1.58647800	-1.37806900	-0.02065000	N	-0.24168000	0.95713500	-0.86938500
H	-3.13337600	-3.54898400	2.63832100	N	-0.62670300	-1.41199100	1.68615900	C	-1.64590300	-1.28045600	-0.03685600
C	-2.78069500	-2.69727200	0.64850500	O	-0.39412000	-0.02132500	-1.76094700	N	0.57691400	-1.58006900	-1.64767300
H	-3.99764500	-3.18967300	0.06614600	N	-0.94755700	-2.61640400	-1.00868000	C	0.28599200	-0.03575700	1.72690700
C	-4.29218400	-2.94424200	-1.27209100	C	-2.01078200	-2.01860600	1.77032800	H	0.67959900	-2.44455800	1.05422000
H	-5.22463900	-3.32563600	-1.71658100	C	-2.99157700	-1.08533800	1.07088400	C	2.88439700	-1.33439400	-0.88602600
C	-3.36777000	-2.20519700	-2.07562400	H	-4.38600900	-1.16168000	1.33898300	C	4.28960600	-1.46223000	-1.06479700
H	-3.59146400	-2.03147200	-3.14021800	N	-5.24709000	-0.29948300	0.66464600	C	5.13463000	-0.57380100	-0.40808900
C	-2.18190300	-1.70032100	-1.53954500	C	-4.71852700	0.68289700	-0.23133700	H	4.57882600	0.48946200	0.37030400
H	-1.47271500	-1.15014100	-2.16855100	C	-5.00008800	2.62177200	-1.71045100	C	5.40752400	1.47941500	0.99983000
C	-1.86226800	-1.91592300	-0.16093200	C	-3.58028800	2.68769300	-1.87811000	C	4.83574200	2.54317200	1.69277200
H	-2.73428700										

6. DFT Coordinates

H 1.66976600 -0.19317200 -2.85955200
H -0.43714400 1.46087700 -4.24770600
H -1.55185000 3.61028100 -3.49711100
H -2.32852700 5.05252300 -1.65068700
H -2.63425300 5.47753100 0.81403000
H -1.81123900 3.76336600 2.47748600
H -0.71137700 1.67904000 1.71779600
H -0.33742100 -3.48002800 -1.35811100
H -0.73627000 -2.73172500 -2.93740700
H -3.18547500 -2.73731300 -2.72165900
H -5.24975500 -1.87737200 -1.52574600
H -6.24504600 -0.79115200 0.48867100
H -5.95679300 0.24156100 2.76659100
H -3.64491400 0.45824100 3.75425400
H -1.63451200 -0.25723100 2.46264500
C 0.82586900 -3.41584200 1.68670900
C 1.01853900 -6.46398500 2.46671100
H 1.94251200 -5.15500700 2.12640500
H 1.11231000 -3.38482500 3.54136800
H 0.14673500 -5.31425100 2.32088900

Coordinates of S = 1 $[\text{Fe}^{\text{IV}}(\text{O})(\text{BQPA})\text{NCCH}_3]^{2+}$:

Fe -0.00032500 0.41508300 -0.29087000
N -0.00094500 2.22010700 -1.10058300
O 0.00009900 -0.25943600 -1.79317400
C -0.00040800 0.17128800 2.66599000
N -0.00034000 1.27491100 1.61270300
C 1.25152700 2.11051100 1.69003500
C -1.25225400 2.11043700 1.68998200
C -2.38800700 1.34139300 1.03252300
C -3.72682800 1.53590100 1.47322900
C -4.74976300 0.82942600 0.85314100
C -4.43829400 -0.08201600 -0.20228000
C -3.05278700 -0.23546700 -0.61544700
N -2.04310000 0.50392600 0.02251900
H -3.92174400 2.23153900 2.30210800
H -5.79669700 0.94997200 1.17472400
C -5.46342600 -0.85182000 -0.84979800
C -2.75728200 -1.15946400 -1.66865800
C 2.38746600 1.34164700 1.03268600
C 3.72615700 1.53609300 1.47381000
C 4.74931500 0.82994500 0.85371600
C 4.43821800 -0.08097900 -0.20225900
C 3.05284300 -0.23431100 -0.61591300
N 2.04290500 0.50460200 0.02221200
H 3.92080400 2.23141300 2.30301900
H 5.79614400 0.95040200 1.17567300
C 5.46360100 -0.85032100 -0.84992900
C 2.75773900 -1.15761000 -1.66984800
C -5.14323800 -1.74596100 -1.86705200
H -6.50557400 -0.71671400 -0.51874300
C -3.78011900 -1.89195300 -2.27428000
H -1.72252000 -1.26360600 -0.21169500
H -5.93133300 -2.33622900 -2.35985000
H -3.52759600 -2.59471000 -3.08419200
H 1.72308700 -1.26157200 -2.01329100
C 3.78081500 -1.88963800 -2.27562000
C 5.14379200 -1.74384400 -1.86784500
H 6.50564000 -0.71532800 -0.51848300
H 3.52859900 -2.59185600 -3.08609600
H 5.93208100 -2.33374600 -2.36077000
H 1.49172000 2.38524600 2.73835700
H -1.49256600 2.38513100 2.73829200
H -1.07919400 3.05136900 1.12918000
H 1.07844800 3.05142000 1.12919100
C 0.00120900 -2.52214300 0.07744900
C 0.00041700 -1.21909400 0.04700600
C 0.00189100 -3.71380000 0.81654500
H 0.00124500 -2.51207900 -1.01900700
C 0.00108900 -2.37949100 2.84819200
C 0.00181900 -3.64304000 2.22739000
H 0.00247500 -4.67709400 0.28694100
H 0.00104500 -2.27870600 3.94384600
H 0.00234800 -4.56027400 2.83554200
N 0.00044600 -1.29776300 0.68456500
H 0.88890600 0.28535300 3.31903000
H -0.89050100 0.28463200 3.31809100
C -0.00123600 3.21307000 -1.71636700
C -0.00167900 4.46971500 -2.47440200
H -0.00126200 4.24249300 -3.56032700
H -0.90901500 5.05442500 -2.21795500
H 0.90490900 5.05536500 -2.21745300

Coordinates of S = 2 $[\text{Fe}^{\text{IV}}(\text{O})(\text{BQPA})\text{NCCH}_3]^{2+}$:

C 3.12650400 -0.43628200 0.55926400
C 4.51688500 -0.23518700 0.62026400
C 5.18459200 0.26904100 -0.51667200
C 4.44068900 0.56247300 -1.67957200
C 3.05079900 0.35020200 -1.67083600
N 2.41277400 -0.14110400 -0.57311500
H 5.05983000 -0.47098600 1.54728400
H 6.27227800 0.43546800 -0.49134700
H 4.92162900 0.95846400 -2.58541900
H 2.40801700 0.56370600 -2.53613800
C 0.52745200 1.99902000 1.19791000
C 0.47418300 3.36217800 1.55269400
C 0.20032700 4.32044500 0.55836600
C -0.00465700 3.88973400 -0.77147300
C 0.06404300 2.51881500 -1.05892300
C 0.31624300 1.59172200 -0.08677300
H 0.64898000 3.65522600 2.59847800
H 0.15280800 5.38945500 0.81578200
H -0.21305700 4.60179600 -1.58267300
H -0.07152600 2.11782200 -2.07176100
C -1.49617600 -1.02914700 1.57661800
C -2.69361200 -1.21302300 2.32255100
C -3.91158400 -0.89041600 1.73475500
C -3.93951300 -0.37224500 0.40314500
C -2.68487500 -0.20677300 -0.31074500
C -1.47473600 -0.55245800 0.30604100
H -2.63011900 -1.59627700 3.35216100
H -4.85589800 -1.01545100 2.28834000
C -5.17206600 -0.00493900 -0.23646000
C -2.71732600 0.32039600 -1.64157700
H -1.77822100 0.42331700 -2.19751600
C -3.93461000 0.66738700 -2.23033100
C -5.17236700 0.50935000 -1.52994800
H -6.11244500 -0.13982500 0.32184500
H -3.93925400 1.06869800 -3.25627500
H -6.11873000 0.791133800 -2.01706500
C -0.65913200 -3.44850000 -0.86243000
C 0.74772400 -4.88334500 -1.15685400
H 1.78693100 -5.23198600 -0.98662500
H 0.46693200 -5.05667000 -2.21620100
H 0.05383300 -5.43929600 -0.49341300

Coordinates of S = 2 $[\text{Fe}^{\text{IV}}(\text{O})(\text{QBPA})\text{NCCH}_3]^{2+}$:

Fe -0.29403100 0.33159000 -0.49403700
N -0.15245000 2.56387700 -0.54010300
O -0.06536600 0.15655700 -2.10327600
C -0.73188200 -0.96646900 2.17864600
H -1.44764400 -1.01962700 3.02375800
H 0.27931800 -1.16567800 2.59114200
N -0.71925800 0.44605200 1.59246600
C 0.41125400 1.24088300 2.21142800
H 0.41097200 1.13588400 3.31684200
H 0.25289600 2.31127200 1.97089700
C -0.205787900 1.14626900 1.75523600
H -1.86904500 2.23832000 1.69484500
H -2.50195500 0.93167300 2.74883300
C -2.99509300 0.771117200 0.61372000
C -4.39593400 0.73415900 0.73173700
C -5.16822800 0.47285000 -0.42189700
C -4.52094200 0.25218800 -1.65756900
C -3.11610900 0.28674500 -1.70018900
N -2.37647600 0.54385600 -0.58659600
H -4.86761900 0.90818100 1.70997000
H -6.26633100 0.43736400 -0.35384400
H -5.08984200 0.04517300 -2.57522300
H -2.53959600 0.10216200 -2.61852300
C -1.01637000 -2.03717600 1.13308400
C -1.52743100 -3.30690400 1.46332600
C -1.64986700 -4.27500100 0.44342500
C -1.26503200 -3.94813800 -0.87633700
C -0.78347000 -2.65392400 -1.13623100
N -0.65928200 -1.72574100 -0.14712400
H -1.81776200 -3.52868800 2.50093900
H -2.04716100 -5.27473900 0.67705000
H -1.34822400 -4.67600300 -1.69609800
H -0.49665600 -2.31280400 -2.14190000
C 1.73579000 0.78513100 1.60368800
C 2.94658700 0.90571500 2.34158200
C 4.14124600 0.50885500 1.74626700
H -0.17133200 -1.32396000 3.29807300
C 4.13350300 -0.03637400 0.42422700
C 2.86509600 -0.14410800 -0.27186700
N 1.68690500 0.29677400 0.33869500
H 2.91716200 1.30412400 3.36611500

6. DFT Coordinates

```
H      5.09547000  0.59299200  2.29085700
C      5.33263600 -0.49230000 -0.22108100
C      2.83724800 -0.72132900 -1.58119700
H      1.87823900 -0.80706700 -2.10819000
C      4.02273600 -1.15784000 -2.17583000
C      5.27944000 -1.04266400 -1.49939700
H      6.28825200 -0.40097700  0.31972800
H      3.98864700 -1.60036500 -3.18402600
H      6.19957100 -1.39379500 -1.99181700
C     -0.07417000  3.70246700 -0.80213800
C      0.02240500  5.13355300 -1.11672300
H     -0.96267100  5.61527600 -0.94863700
H      0.31954700  5.25833600 -2.17818100
H      0.78289700  5.60487700 -0.46084600
```

7. References

1. Petasis, D. T.; Hendrich, M. P., *Methods in Enzymology*, **2015**, Vol 563, (Eds.: P. Z. Qin, K. Warncke), Academic Press, pp 171-208.
2. Bigi, J. P.; Harman, W. H.; Lassalle-Kaiser, B.; Robles, D. M.; Stich, T. A.; Yano, J.; Britt, R. D.; Chang, C. J., A High-Spin Iron(IV)-Oxo Complex Supported by a Trigonal Nonheme Pyrrolide Platform. *J. Am. Chem. Soc.* **2012**, *134*, 1536-1542.
3. England, J.; Guo, Y.; Farquhar, E. R.; Young, V. G., Jr.; Münck, E.; Que, L., Jr., The Crystal Structure of a High-Spin Oxoiron(IV) Complex and Characterization of Its Self-Decay Pathway. *J. Am. Chem. Soc.* **2010**, *132* (25), 8635-8644.
4. Lacy, D. C.; Gupta, R.; Stone, K. L.; Greaves, J.; Ziller, J. W.; Hendrich, M. P.; Borovik, A. S., Formation, Structure, and EPR Detection of a High Spin FeIV—Oxo Species Derived from Either an FeIII—Oxo or FeIII—OH Complex. *J. Am. Chem. Soc.* **2010**, *132*, 12188-12190.
5. Warm, K.; Paskin, A.; Kuhlmann, U.; Bill, E.; Swart, M.; Haumann, M.; Dau, H.; Hildebrandt, P.; Ray, K., A Pseudotetrahedral Terminal Oxoiron(IV) Complex: Mechanistic Promiscuity in C-H bond Oxidation Reactions. *Angew. Chem. Int. Ed.* **2021**, *60*, 6752-6756.
6. Dong, Y.; Fujii, H.; Hendrich, M. P.; Leising, R. A.; Pan, G.; Randall, C. R.; Wilkinson, E. C.; Zang, Y.; Que, L., Jr.; Fox, B. G.; Kauffmann, K.; Münck, E., A High-Valent Nonheme Iron Intermediate. Structure and Properties of $[\text{Fe}_2(\mu\text{-O})_2(5\text{-Me-TPA})_2](\text{ClO}_4)_3$. *J. Am. Chem. Soc.* **1995**, *117*, 2778-2792.
7. Tanga, M. J.; Bupp, J. E.; Tochimoto, T. K., Syntheses of five potential heterocyclic amine food mutagens. *J. Heterocycl. Chem.* **1997**, *34* (3), 717-727.
8. Stock, N. S.; Bain, G.; Zunic, J.; Li, Y.; Ziff, J.; Roppe, J.; Santini, A.; Darlington, J.; Prodanovich, P.; King, C. D.; Baccei, C.; Lee, C.; Rong, H.; Chapman, C.; Broadhead, A.; Lorrain, D.; Correa, L.; Hutchinson, J. H.; Evans, J. F.; Prasit, P., 5-Lipoxygenase-Activating Protein (FLAP) Inhibitors. Part 4: Development of 3-[3-tert-Butylsulfanyl-1-[4-(6-ethoxypyridin-3-yl)benzyl]-5-(5-methylpyridin-2-ylmethoxy)-1H-indol-2-yl]-2,2-dimethylpropionic Acid (AM803), a Potent, Oral, Once Daily FLAP Inhibitor. *J. Med. Chem.* **2011**, *54* (23), 8013-8029.
9. Zang, Y.; Kim, J.; Dong, Y.; Wilkinson, E. C.; Appelman, E. H.; Que, L., Models for Nonheme Iron Intermediates: Structural Basis for Tuning the Spin States of Fe(TPA) Complexes. *Journal of the American Chemical Society* **1997**, *119* (18), 4197-4205.
10. Chen, K.; Que, L., Stereospecific Alkane Hydroxylation by Non-Heme Iron Catalysts: Mechanistic Evidence for an FeVO Active Species. *J. Am. Chem. Soc.* **2001**, *123* (26), 6327-6337.
11. Biswas, A. N.; Puri, M.; Meier, K. K.; Oloo, W. N.; Rohde, G. T.; Bominaar, E. L.; Münck, E.; Que, L., Modeling TauD-J: A High-Spin Nonheme Oxoiron(IV) Complex with High Reactivity toward C–H Bonds. *J. Am. Chem. Soc.* **2015**, *137* (7), 2428-2431.
12. Rasheed, W.; Draksharapu, A.; Banerjee, S.; Young, V. G.; Fan, R.; Guo, Y.; Ozerov, M.; Nehrkorn, J.; Krzystek, J.; Telser, J.; Que, L., Crystallographic Evidence for a Sterically Induced Ferryl Tilt in a Non-Heme Oxoiron(IV) Complex that Makes it a Better Oxidant. *Angew. Chem. Int. Ed.* **2018**, *57* (30), 9387-9391.
13. Lubben, M.; Meetsma, A.; Wilkinson, E. C.; Feringa, B.; Que Jr, L., Nonheme Iron Centers in Oxygen Activation: Characterization of an Iron(III) Hydroperoxide Intermediate. *Angew. Chem. Int. Ed.* **1995**, *34* (13-14), 1512-1514.
14. Lim, M. H.; Rohde, J.-U.; Stubna, A.; Bukowski, M. R.; Costas, M.; Ho, R. Y. N.; Münck, E.; Nam, W.; Que, L., Jr., An $\text{Fe}^{\text{IV}}=\text{O}$ Complex of a Tetradentate Tripodal Nonheme Ligand. *Proc. Natl. Acad. Sci. USA* **2003**, *100* (7), 3665-3670.
15. Biswas, A. N.; Puri, M.; Meier, K. K.; Oloo, W. N.; Rohde, G. T.; Bominaar, E. L.; Münck, E.; Que, L., Modeling TauD-J: A High-Spin Nonheme Oxoiron(IV) Complex with High Reactivity toward C–H Bonds. *J. Am. Chem. Soc.* **2015**, *137* (7), 2428-2431.
16. Zang, Y.; Kim, J.; Dong, Y.; Wilkinson, E. C.; Appelman, E. H.; Que, L., Models for Nonheme Iron Intermediates: Structural Basis for Tuning the Spin States of Fe(TPA) Complexes. *J. Am. Chem. Soc.* **1997**, *119* (18), 4197-4205.
17. Chen, K.; Que, L., Stereospecific Alkane Hydroxylation by Non-Heme Iron Catalysts: Mechanistic Evidence for an FeVO Active Species. *Journal of the American Chemical Society* **2001**, *123* (26), 6327-6337.

18. Klinker, E. J.; Kaizer, J.; Brennessel, W. W.; Woodrum, N. L.; Cramer, C. J.; Que, L., Jr., Structures of Nonheme Oxoiron(IV) Complexes from X-ray Crystallography, NMR Spectroscopy, and DFT Calculations. *Angew. Chem. Int. Ed.* **2005**, *44* (24), 3690-3694.
19. Biswas, A. N.; Puri, M.; Meier, K. K.; Oloo, W. N.; Rohde, G. T.; Bominaar, E. L.; Münck, E.; Que, L., Jr., Modeling TauD-J: A High-Spin Nonheme Oxoiron(IV) Complex with High Reactivity Toward C-H Bonds. *J. Am. Chem. Soc.* **2015**, *137* (7), 2428-2431.
20. Rasheed, W.; Draksharapu, A.; Banerjee, S.; Young Victor, G.; Fan, R.; Guo, Y.; Ozerov, M.; Nehrkorn, J.; Krzystek, J.; Telser, J.; Que, L., Crystallographic Evidence for a Sterically Induced Ferryl Tilt in a Non-Heme Oxoiron(IV) Complex that Makes it a Better Oxidant. *Angew. Chem. Int. Ed.* **2018**, *(0)*, DOI: 10.1002/anie.201804836.
21. Banerjee, S.; Rasheed, W.; Fan, R.; Draksharapu, A.; Oloo, W. N.; Guo, Y.; Que, L., Jr., NMR Reveals That a Highly Reactive Nonheme Fe(IV)=O Complex Retains its 6-Coordinate Geometry and S = 1 State in Solution. *Chem. Eur. J.* **2019**, *25*, 9608-9613.
22. Neese, F., Prediction and interpretation of the ^{57}Fe isomer shift in Mössbauer spectra by density functional theory. *Inorg. Chim. Acta* **2002**, *337*, 181-192.
23. Frisch, M. J.; Trucks, G. W.; Schlegel, H. B.; Scuseria, G. E.; Robb, M. A.; Cheeseman, J. R.; Scalmani, G.; Barone, V.; Petersson, G. A.; Nakatsuji, H.; Li, X.; Caricato, M.; Marenich, A. V.; Bloino, J.; Janesko, B. G.; Gomperts, R.; Mennucci, B.; Hratchian, H. P.; Ortiz, J. V.; Izmaylov, A. F.; Sonnenberg, J. L.; Williams-Young, D.; F. Ding, F. L.; Egidi, F.; Goings, J.; Peng, B.; Petrone, A.; Henderson, T.; Ranasinghe, D.; Zakrzewski, V. G.; J. Gao, N. R.; Zheng, G.; Liang, W.; Hada, M.; Ehara, M.; Toyota, K.; Fukuda, R.; Hasegawa, J.; Ishida, M.; Nakajima, T.; Honda, Y.; Kitao, O.; Nakai, H.; Vreven, T.; Throssell, K.; Jr., J. A. M.; Peralta, J. E.; Ogliaro, F.; Bearpark, M. J.; Heyd, J. J.; Brothers, E. N.; Kudin, K. N.; Staroverov, V. N.; Keith, T. A.; Kobayashi, R.; Normand, J.; Raghavachari, K.; Rendell, A. P.; Burant, J. C.; Iyengar, S. S.; Tomasi, J.; Cossi, M.; Millam, J. M.; Klene, M.; Adamo, C.; Cammi, R.; Ochterski, J. W.; Martin, R. L.; Morokuma, K.; Farkas, O.; Foresman, J. B.; Fox, D. J., *Gaussian, Inc., Wallingford CT*, 2016.
24. Becke, A. D., Density-functional exchange-energy approximation with correct asymptotic behavior. *Phys. Rev. A Gen. Phys.* **1988**, *38* (6), 3098-3100.
25. Lee, C.; Yang, W.; Parr, R. G., Development of the Colle-Salvetti correlation-energy formula into a functional of the electron density. *Phys. Rev. B Condens. Matter* **1988**, *37* (2), 785-789.
26. Miehlich, B.; Savin, A.; Stoll, H.; Preuss, H., Results obtained with the correlation energy density functionals of becke and Lee, Yang and Parr. *Chem. Phys. Lett.* **1989**, *157* (3), 200-206.
27. Tomasi, J.; Mennucci, B.; Cammi, R., Quantum Mechanical Continuum Solvation Models. *Chem. Rev.* **2005**, *105* (8), 2999-3094.
28. Grimme, S.; Antony, J.; Ehrlich, S.; Krieg, H., A consistent and accurate ab initio parametrization of density functional dispersion correction (DFT-D) for the 94 elements H-Pu. *J. Chem. Phys.* **2010**, *132* (15), 154104.
29. Borgogno, A.; Rastrelli, F.; Bagno, A., Characterization of Paramagnetic Reactive Intermediates: Predicting the NMR Spectra of Iron(IV)-Oxo Complexes by DFT. *Chem. Eur. J.* **2015**, *21* (37), 12960-12970.
30. Borgogno, A.; Rastrelli, F.; Bagno, A., Predicting the spin state of paramagnetic iron complexes by DFT calculation of proton NMR spectra. *Dalton Trans.* **2014**, *43* (25), 9486-9496.
31. Rastrelli, F.; Bagno, A., Predicting the ^1H and ^{13}C NMR spectra of paramagnetic Ru(III) complexes by DFT. *Magn. Reson. Chem.* **2010**, *48* (S1), S132-S141.
32. Rastrelli, F.; Bagno, A., Predicting the NMR Spectra of Paramagnetic Molecules by DFT: Application to Organic Free Radicals and Transition-Metal Complexes. *Chem. Eur. J.* **2009**, *15* (32), 7990-8004.
33. Bertini, I.; Luchinat, C.; Parigi, G., Magnetic susceptibility in paramagnetic NMR. *Prog. Nucl. Magn. Reson. Spectrosc.* **2002**, *40* (3), 249-273.
34. Bertini, I.; Luchinat, C.; Parigi, G., Solution NMR of Paramagnetic Molecules: Applications to Metallobiomolecules and Models. *Elsevier* **2001**, *Solution NMR of Paramagnetic Molecules: Applications to Metallobiomolecules and Models*.
35. Hrobárik, P.; Reviakine, R.; Arbuznikov, A. V.; Malkina, O. L.; Malkin, V. G.; Köhler, F. H.; Kaupp, M., Density functional calculations of NMR shielding tensors for paramagnetic systems with arbitrary spin multiplicity: Validation on 3d metallocenes. *J. Chem. Phys.* **2007**, *126* (2), 024107.

